

AD-A263 207



2

PL-TR-92-2202

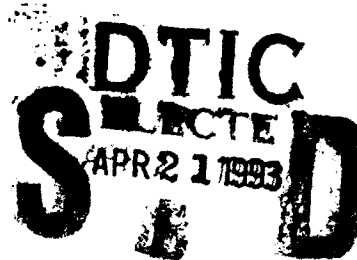
SIO Ref 92-22
MPL-U-65/92

**AN AUTOMATED OBSERVING SYSTEM FOR
PASSIVE EVALUATION OF CLOUD COVER AND VISIBILITY**

J. E. Shields
R. W. Johnson
M. E. Karr

University of California, San Diego
Marine Physical Laboratory
San Diego, CA 92152-6400

July 1992



Final Report
September 1988 - January 1992

APPROVED FOR PUBLIC RELEASE; DISTRIBUTION UNLIMITED

917400
93-08481

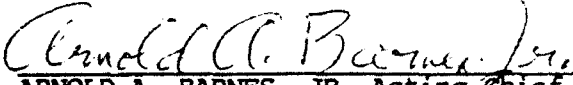


PHILLIPS LABORATORY
Directorate of Geophysics
AIR FORCE MATERIEL COMMAND
HANSCOM AIRFORCE BASE, MA 01731-5000

93 4 20 102

"This technical report has been reviewed and is approved for publication"


HENRY A. BROWN
Contract Manager


ARNOLD A. BARNES, JR. Acting Chief
Atmospheric Structure Branch


ROBERT A. MCCLATCHEY, Director
Atmospheric Sciences Division

This report has been reviewed by the ESC Public Affairs Office (PA) and is releasable to the National Technical Information Service (NITS).

Qualified requesters may obtain additional copies from the Defense Technical Information Center. All others should apply to the National Technical Information Service.

If your address has changed, or if you wish to be removed from the mailing list, or if the addressee is no longer employed by your organization, please notify PL/IMA, Hanscom AFB, MA 01731-5000. This will assist us in maintaining a current mailing list.

Do not return copies of this report unless contractual obligations or notices on a specific document requires that it be returned.

REPORT DOCUMENTATION PAGE

Form Approved
OMB No. 0704-0188

Public reporting burden for this collection of information is estimated to average 1 hour per response, including the time for reviewing instructions, searching existing data sources, gathering and maintaining the data needed, and completing and reviewing the collection of information. Send comments regarding this burden estimate or any other aspect of this collection of information, including suggestions for reducing this burden, to Washington Headquarters Services, Directorate for Information Operations and Reports, 1215 Jefferson Davis Highway, Suite 1204, Arlington, VA 22202-4302, and to the Office of Management and Budget, Paperwork Reduction Project (0704-188), Washington, DC 20503.

1. Agency Use Only (Leave blank).		2. Report Date. July 1992		3. Report Type and Dates Covered. Final Report, Sept. 1988 - Jan. 1992	
4. Title and Subtitle. An Automated Observing System for Passive Evaluation of Cloud Cover and Visibility				5. Funding Numbers. Program Element No. F19628-88-C-0154 63707F Project No. 2688 Task No. 03 Accession No. HA	
6. Author(s). J. E. Shields R. W. Johnson M. E. Karr				8. Performing Organization Report Number. SIO Re1 92-22 MPL-U-65/92	
7. Performing Organization Name(s) and Address(es). University of California, San Diego Marine Physical Laboratory San Diego, CA 92093-0701				10. Sponsoring/Monitoring Agency Report Number. PL-TR-92-2202	
9. Sponsoring/Monitoring Agency Name(s) and Address(es). Phillips Laboratory Hanscom AFB, MA 01731-5000 Contract Manager: Dr. H. A. Brown/GPAA					
11. Supplementary Notes.					
12a. Distribution/Availability Statement. Approved for public release, distribution unlimited.				12b. Distribution Code.	
13. Abstract (Maximum 200 words). The Automated Observing System is a passive system for determination of cloud cover and sector visibility. This system was developed from related systems, the Whole Sky Imager for cloud field assessment, and the Horizon Scanning Imager for determination of the sector visibility. During the past funding interval, much of the effort on this system was directed toward development of night visibility capability. This report discusses the theoretical development of the equations and analytic approaches to night visibility. A variety of hardware and software adaptations are discussed, which allow the sensor to utilize multiple integration periods for increased system sensitivity. Sample results are included. Secondary developments discussed in this report include an in-depth sensitivity analysis of the daytime visibility system, as well as achievement of more accurate cloud algorithms and night cloud capability funded separately. This is followed by recommendations for improvements to the current system, and for development of tactical systems based on the existing capability.					
14. Subject Terms. Visibility, Contrast Transmittance, Atmosphere, Sector Visibility, Weather Sensors, Aviation Weather Observations, Weather, Atmospheric Visibility, Cloud, Cloud Cover, Cloud Free Line of Sight				15. Number of Pages. 40	
				16. Price Code.	
17. Security Classification of Report. Unclassified	18. Security Classification of This Page. Unclassified	19. Security Classification of Abstract. Unclassified	20. Limitation of Abstract. SAR		

Summary

The Automated Observing System is a passive system for determination of cloud cover and sector visibility. This system was developed from related systems, the Whole Sky Imager for cloud field assessment, and the Horizon Scanning Imager for determination of the sector visibility. During the past funding interval, much of the effort on this system was directed toward development of night visibility capability. This report discusses the theoretical development of the equations and analytic approaches to night visibility. A variety of hardware and software adaptations are discussed, which allow the sensor to utilize multiple integration periods for increased system sensitivity. Sample results are included. Secondary developments discussed in this report include an in-depth sensitivity analysis of the daytime visibility system, as well as achievement of more accurate cloud algorithms and night cloud capability funded separately. This is followed by recommendations for improvements to the current system, and for development of tactical systems based on the existing capability.

DISC QUALITY CONTROLLED 1

Accession For	
NTIS GRA&I	<input checked="checked" type="checkbox"/>
DTIC TAB	<input type="checkbox"/>
Unannounced	<input type="checkbox"/>
Justification	
By _____	
Distribution/	
Availability Codes	
Dist	Avail and/or Special
A-1	

TABLE OF CONTENTS

Summary.....	iii
List of Illustrations & Tables.....	vi
1. Introduction.....	1
2. The Composite HSI/WSI Observing Station.....	1
2.1 The Daytime HSI.....	1
2.2 The Daytime WSI.....	2
2.3 The As-built Composite HSI/WSI.....	3
3. Visibility at Night.....	4
3.1 Definitions of Visibility at Night.....	4
3.1.1 Basis for the defining equations.....	4
3.1.2 Comparison with Koschmieder Visibility.....	5
3.1.3 Common Usage of the Visibility Equations.....	5
3.2 Measuring the Optical Attenuation at Night.....	8
3.2.1 Absolute Measurement Approach.....	9
3.2.2 Relative Measurement Approach.....	9
3.2.3 Summary of the Visibility Equations.....	10
3.2.4 Conversion to Point Sources.....	10
3.3 Hardware Adaptations for Visibility at Night.....	11
3.3.1 CID Injection Inhibit.....	11
3.3.2 VS-100 Image Board.....	11
3.3.3 The Integration Control Circuit.....	12
3.3.4 The Auto-iris Inhibit.....	12
3.4 Software Adaptations for Visibility at Night.....	12
3.4.1 Night HSI Programs.....	12
3.4.2 Adaptation of the Day HSI/WSI Programs for VS-100.....	13
3.5 CID Camera Behavior under Integration.....	13
3.6 Sample Night Visibility Computations.....	15
4. Daytime System Refinements.....	18
4.1 Changes to the HSI/WSI Programs.....	18
4.2 Sensitivity Study of Daytime Visibility.....	19
4.2.1 Summary of the Sensitivity Study.....	19
4.2.2 Recommendations Relating to Measurement Accuracy.....	19
4.2.3 Recommendations Relating to Non-ideal Conditions.....	22
4.3 Recommended Change to the HSI Visibility Equation.....	23
4.3.1 Derivation of the Koschmieder Equation.....	23
4.3.2 Determining Visibility from Measured Apparent Contrast.....	24
4.3.3 Relationship between the Proposed and Current Equation.....	25
5. Related Studies.....	25
5.1 Directional Cloud Decision Algorithm.....	26
5.2 Development of the Day/Night WSI.....	29
6. Recommendations.....	27
6.1 Compact and Ruggedized Systems.....	29
6.1.1 A Compact WSI System.....	29
6.1.2 A Compact HSI System.....	30
6.2 Improvements of Quality and Capability of the Current HSI/WSI.....	31
6.2.1 Integration of the Sensitivity Study Results.....	31
6.2.2 Addition of the Directional Algorithm.....	31
6.2.3 Further Development of Night Visibility.....	31
6.3 A 220 Degree Whole Sky Imager.....	31
7. Summary.....	32
8. Acknowledgments.....	32
9. References.....	32

LIST OF ILLUSTRATIONS

Fig. #	Figure Title	Page
1	Sample Visibility Image.....	1
2	Apparent Contrast vs. Range.....	2
3	HSI Procedural Flow Chart.....	2
4	Cloud Decision Image.....	3
5	WSI Basic Image Processing Flow Chart.....	3
6	Composite HSI/WSI As-built Field Installation.....	4
7	Composite HSI/WSI Accessory Control Panel.....	4
8	Koschmieder Visibility and Transmissometer Night Visibility as a Function of Extinction Coefficient.....	6
9	Transmissometer Night Visibility as a Function of Koschmieder Visibility.....	7
10	Visibility Equation Usage.....	8
11	Defining Equation Relations for HSI Visibility.....	10
12	Conceptual Illustration of output RS170 Video Signal (Vertical frame rate) at various injection inhibit settings.....	12
13	Results of the Linearity Calibration, showing the slight non-linearity of the CID Sensor at 0 Integration.....	14
14	Results of the Calibration showing camera response to increasing the injection inhibit setting (increasing the integration period).....	16
15	Error in visibility due to system or input errors, when $C_o = .8$ and $L_q = 200$	20
16	Error in visibility due to system or input errors, when $C_o = .5$ and $L_q = 200$	21
17	Clear Sky Solar Zenith Angle Dependence: 11/Feb/89 - Columbia, MO.....	26
18	Clear Sky Haze Layer Dependence: Columbia, MO, 1989.....	26
19	Variable threshold cloud decision image.....	27
20	Natural Illumination Levels.....	28
21	Sample Night Sky Images from the Day/Night WSI.....	29
	a. Starlight (no moon) conditions 11 Sep 91, 25 seconds integration	
	b. Moonlight conditions. 18 Sep 91, 30 seconds integration	

LIST OF TABLES

Table #	Table Title	Page
1	Visibility Sample Values.....	15
2	Computation of Inherent Signal from Clear Night Data (16 Jan).....	17
3	Computation of Foggy Night Visibility (23 Jan) Using Absolute Equation.....	17
4	Computation of 23 Jan Visibility Using Relative Equation.....	18

1. INTRODUCTION

In recent years the Marine Physical Laboratory of Scripps Institution of Oceanography has developed and fielded several imaging systems for assessment of the cloud field dynamics, as well as for visibility determination. The Whole Sky Imager (WSI) images the sky dome and identifies cloud distributions, from which earth-to-space cloud free line of sight, cloud free arc, and cloud cover determinations may be made. The Horizon Scanning Imager (HSI) images scenes near the horizon, with a small field of view lens and near-photopic filtering, for determining the visibility over extended paths.

Both of these units have been combined and adapted for near-real time assessments, in the Automated Observing System (AOS) stationed at Otis ANGB. This work has been reported previously in GL-TR-89-0061, Johnson, et al, (1989), and PL-TR-91-2016(I), Johnson, et al (1990), and PL-TR-91-2216, Johnson, et al (1991).

During the past year, work has continued to upgrade the performance of the daytime HSI system, and extend the HSI capability to the nighttime regime. This final report discusses this work, as well as summarizing recommended upgrades to the AOS system.

2. THE COMPOSITE HSI/WSI OBSERVING STATION

The composite HSI/WSI observing station includes a daytime-capable HSI, and day-time capable WSI. In addition, the HSI hardware and software capabilities have been extended to be night-capable, i.e. provide capability for determining visibility at night, although the night capability is not fully automated at this time. A night-capable WSI unit, for measurement of cloud fields at night, has been developed under separate contract, and is a reasonable candidate for inclusion in the observing station at a later point in time.

This section will provide a summary overview of the daytime HSI and WSI components. The Night HSI will be discussed further in later sections.

2.1 The Daytime HSI

The Horizon Scanning Imager uses a solid state Charge Injection Device (CID) sensor for the acquisition of 512 x 480 images of the horizon. The use of a 5 degree field of view lens, in combination with an auto-iris and a spectral filter (green, with a peak wavelength of 550 nm, and a passband of 70 nm), allows the acquisition of high resolution near-photopic images. A precision rotary table is used for highly reproducible scene acquisition around the horizon.

Dark targets are previously identified in the scene at a variety of ranges. A sample visibility image is shown in Fig. 1. In this scene, the relative radiance of each of these targets is determined, along with the relative radiance of the horizon at the same azimuth. From these determinations, the apparent contrast of each target with respect to the horizon, C_r , is determined.

$$C_r = \frac{L_r - L_b}{L_b} \quad (2.1)$$

where

L_r = Apparent target radiance

L_b = Apparent background radiance



Fig. 1 Sample Visibility Image. Image was acquired with the HSI, and resulting visibility computations are performed automatically in the field.

Figure 2 illustrates the decrease in contrast of a black target with respect to the horizon, as range to the target increases. Note that the apparent contrast, i.e. the contrast as measured from a given range, decreases exponentially. This rate of decrease depends on the attenuation coefficient of the atmosphere. Visibility may be defined as the range at which this contrast decreases to the human contrast threshold, taken to be .05 in this illustration.

The lower curves of Fig. 2 shows the apparent contrast of sample targets which are not perfectly black (inherent radiance not equal to -1). The HSI is able to measure the contrast of non-ideal targets such as represented by the lower curves, at a variety of ranges, and mathematically determine the visibility. The resulting equation discussed in detail in Johnson, et al, (1989), is given below.

$$V = r \ln\left(\frac{\epsilon}{C_o}\right) / \ln\left(\frac{C_r}{C_o}\right) \quad (2.2)$$

This technique has several advantages over visual determination of the visibility. It can use targets which are not black, which are not at a range equal to visibility, and which are not physically adjacent to the horizon. In common practice, the weather observer is forced to use targets with these limitations, to varying degrees, but is unable to rigorously compensate for the non-ideal conditions.

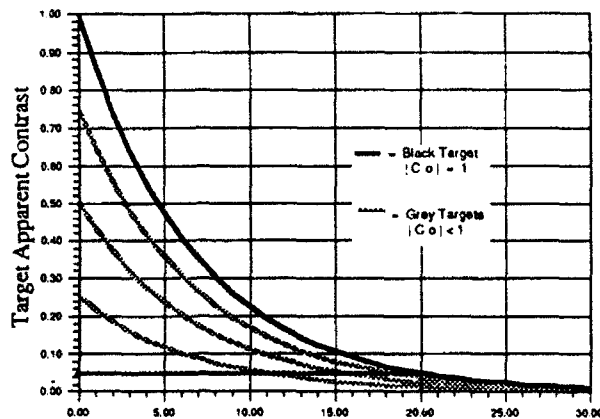


Figure 2 Apparent Contrast vs. Range. Visibility may be defined as the range at which the apparent contrast of the ideal target drops to the human visual threshold, shown as .05 in this illustration.

In comparison with point scatter meters and transmissometers, the HSI has the advantage of using a long path to the target, which yields a much more representative determination. The ability to measure sector visibility, i.e. the variance around the horizon, is also important for many applications.

The basic functional characteristics of the HSI system have remained essentially as described in Johnson, et al, (1989). The general concept of its operational sequence is illustrated in Fig. 3. The diagram has of course been simplified for clarity and does not include the myriad of housekeeping and control details that enable the automatic image acquisition sequences.

The HSI continues to operate reliably, with reasonable accuracy. This year's upgrades to the daytime visibility capability are discussed in Section 4.

2.2 The Daytime WSI

Like the HSI, the Whole Sky Imager is a passive, ground-based sensor. It uses a fisheye lens to acquire images of the upper hemisphere down to an 80 degree zenith angle. A combination of spectral and neutral density filters, in conjunction with a CID camera, enables acquisition of images which may be fully calibrated radiometrically. The 512 x 480 image resolution yields a 1/3 degree spatial resolution in object space, for a footprint of roughly 17 meters for a cloud layer at 3 km altitude.

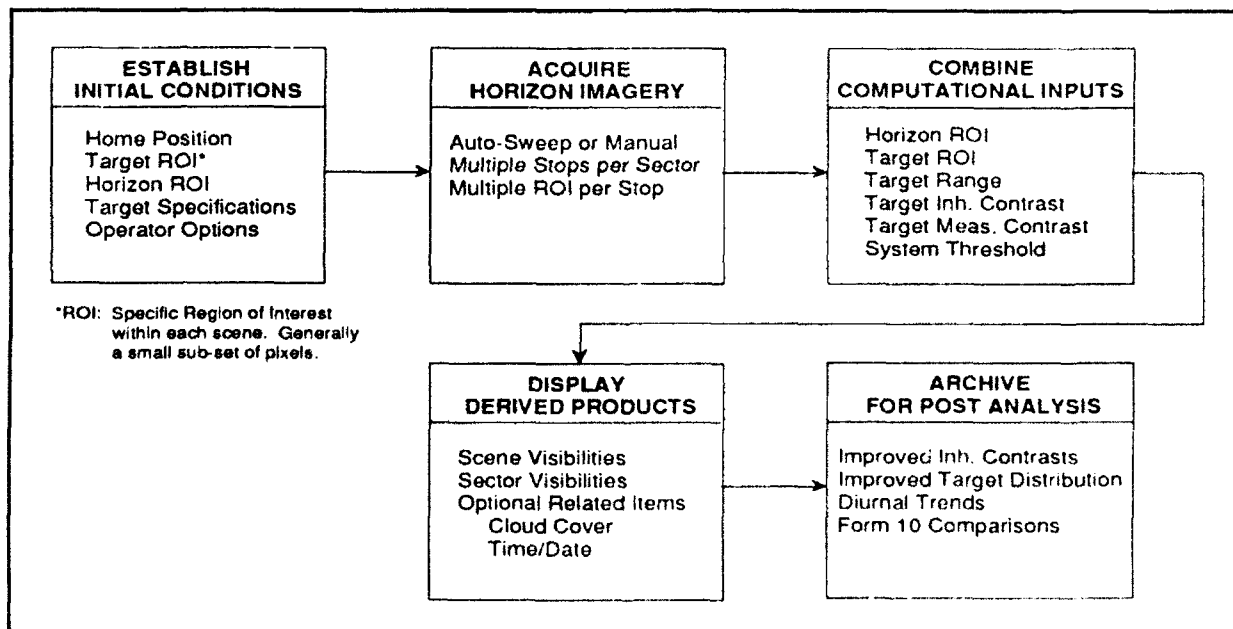


Fig. 3 HSI Procedural Flow Chart

The cloud data undergo several processing steps to yield a final cloud decision image, in which areas identified as opaque cloud are displayed as white, thin cloud are displayed as yellow, and no cloud (clear) are displayed with blue. Data which are not valid due to conditions such as offscale dark are also identified and so labeled. In this procedure, a number of calibrations are applied, to account for slight sensor non-linearities, filter passband differences, neutral density spectral bias, and so on. Images acquired at 650 nm (red) and 450 nm (blue) are ratioed to remove most of the directional and temporal variation in the background sky radiance. In the remaining ratio image, opaque and thin clouds are identified by ratio thresholds, yielding a determination such as shown in Fig. 4.

This ratio technique more fully illustrated in Fig. 5, allows a fully automated determination at each pixel location in the scene. It is significantly more reliable than identification based on the radiance scene, both due to the removal of the directional bias mentioned above, and also because clouds can often be darker than adjacent sky regions.

A further sophistication to the cloud identification scheme uses an angularly dependent clear sky background ratio, normalized by aerosol load or haziness, to correct for the residual directional bias in the ratio image. This technique, developed under separate contract, has not been applied to the composite HSI/WSI system. Its advantages will be discussed in Section 5.

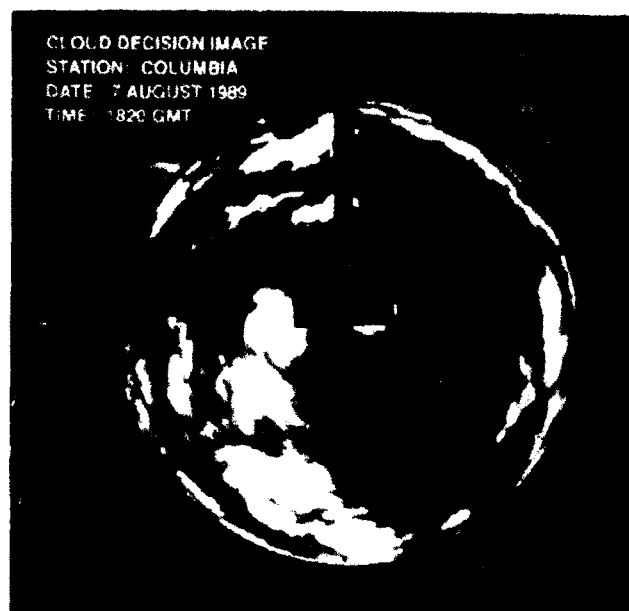


Fig. 4 Cloud Decision Image. Each pixel location has been identified as opaque, thin, or no cloud by an automated algorithm applied to WSI imagery.

2.3 The As-Built Composite HSI/WSI

The as-built HSI/WSI unit is illustrated in Fig. 6. These two separate camera units are controlled by an IBM AT-clone microcomputer with an image board, and a 2.2 Gbyte tape system for data archival. An accessory control panel, illustrated in Fig 7, allows either manual or computer control of the various functions such as filter

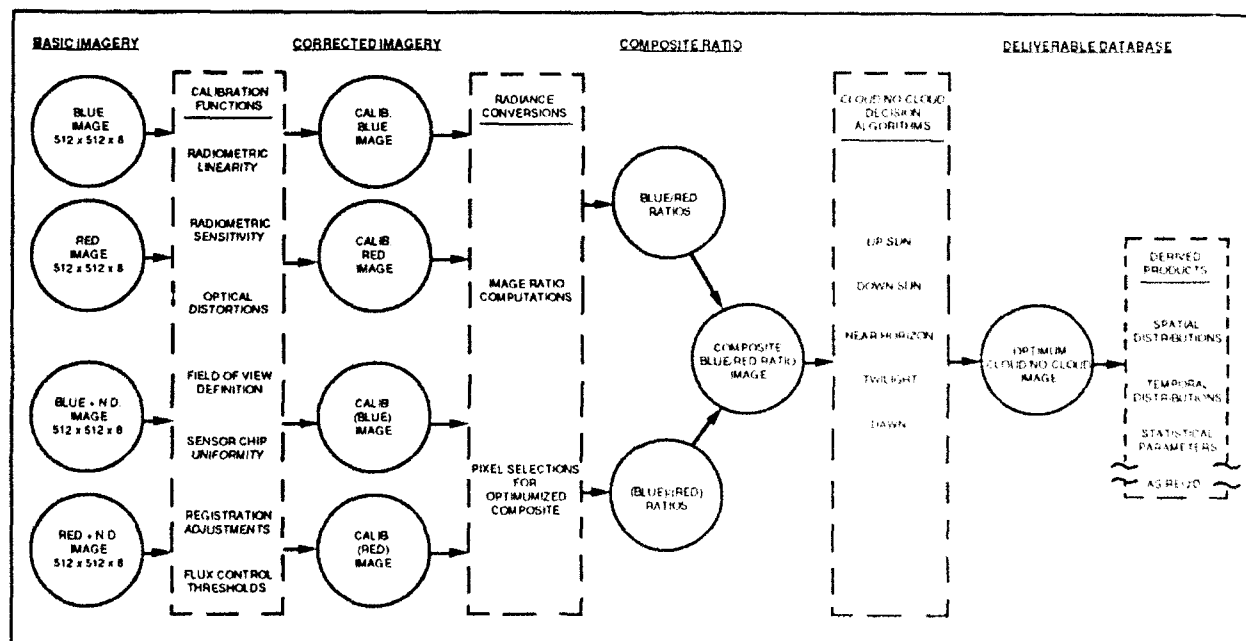


Fig. 5 WSI Basic Image Processing Flow Chart

changer selection, solar occulter angle, rotary table azimuth, and so on.



Fig. 6 Composite HSI/WSI As-built Field Installation

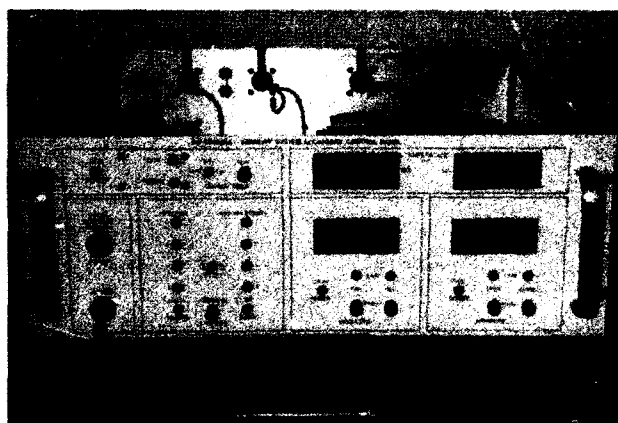


Fig. 7 Composite HSI/WSI Accessory Control Panel

The prototype visibility and cloud detection systems were fabricated as two separate hardware/software entities which need not necessarily be integrated into a single electro-mechanical unit. Each may stand alone and function independently, or if desired, under the control of

the composite HSI/WSI system the two sub-assemblies may be operated jointly under an operator-specified time-share duty cycle.

A nominal automatic duty cycle is for the HSI to run horizon sweeps each minute for eight minutes and every ten minutes insert a cloud cover measurement. In this mode, the system will display its output products of sector visibilities and cloud cover to the CRT display and/or output the data to printer for hardcopy. It will also, at the operator's discretion, archive both original imagery and derived numerical products to its Exabyte tape sub-system for later retrieval and analysis.

3. VISIBILITY AT NIGHT

This section discusses the extension of the HSI capabilities to enable visibility determinations at night. First the theory of visibility at night, and its implication for the HSI algorithms, are discussed. The revision of the HSI hardware is then described. The capabilities and limitations of the CID camera for night time use are discussed, followed by sample calculations.

3.1 Definitions of Visibility at Night

Douglas and Booker (1977) provide an in-depth discussion of visibility at night; a more succinct review is given in Gordon (1989). This section gives a summary of the results.

3.1.1 Basis for the defining equation used with transmissometers

The visibility at night has historically been defined in terms of point sources. A point source with intensity I , in a perfectly transmitting atmosphere, will produce an illuminance E given by

$$E = I / r^2 \quad (3.1)$$

where I is given in candles, and E in lumen/km², or km-candle (Douglas & Booker, p. 2-5). Note that even in clear air, E is a function of range. (The luminance or radiance of extended sources do not decrease as a function of r , in the absence of attenuation.)

In a real atmosphere, there is attenuation which can be characterized by the beam transmittance, defined as the ratio of transmitted to incident flux. The illuminance at range r becomes

$$E = T_r I / r^2 \quad (3.2)$$

where T_r is unitless. The attenuation of the atmosphere can be equally characterized by the transmissivity T (which is the transmittance over unit distance), or the

extinction coefficient σ (which is the rate of change of the flux). These terms are related to transmittance by

$$T_r = T^r = e^{-\sigma r} \quad (3.3)$$

The Federal Meteorological Handbook (1988) defines the visibility as "the greatest distance at which selected objects can be seen and identified," where the visibility markers are defined as "dark or nearly dark objects viewed against the horizon sky during the day, or unfocused lights of moderate intensity (about 25 cd) during the night."

This is a psychophysical definition. Thus at night, using Eq. 3.3, the definition of night visibility might be stated as the distance at which the illuminance reaches a certain psychophysically defined threshold, when the source intensity is 25 candles.

Let night visibility V be the distance at which the illuminance reaches a threshold E_t . Then letting the range $r = V$ in Eq. 3.2, and using Eq. 3.3, the defining equation for night visibility becomes

$$E_t = IT^v / V^2 \quad (3.4)$$

As discussed in Douglas and Booker P. 4-16, this is the most common form of Allard's law, and may be considered as the defining equation for visibility at night.

The problem with this definition is that E_t itself is not well behaved. There is considerable discussion in Douglas and Booker of the best value to use, depending on the exact application. Values of .02 to .052 km candles were measured in fog experiments (Douglas & Booker, p. 4-31). For pilot landing scenarios, tests yielded values ranging from about 2 to 1000 mile candles.

A series of tests was run at Nantucket Island in 1941, comparing transmissometer output with visual sightings. In these tests, the best fit was obtained not by using a constant illuminance threshold, but by using an illuminance threshold which itself is a function of visibility. If S is the threshold obtained at 1 unit distance, this yields a new equation,

$$S / V = IT^v / V^2 \quad (3.5)$$

or

$$S = IT^v / V \quad (3.6)$$

where $S = .052$ for visibility in km, or .084 for visibility in miles when $I = 25$ candle (Douglas & Booker, p. 7-17). This relation in effect states that although the illuminance will still be as shown in Eq. 3.4, the effective illuminance threshold can be much higher in low visibility conditions than in clear air.

Douglas and Booker indicate that this is the relation that has been used in the United States for converting transmissometer values to night visibility since that time. The tables in the current Federal Meteorological Handbook are consistent with Equation 3.6.

Thus whereas Eq. 3.4, Allard's law, is the defining equation, the threshold was found in at least one series of tests to be a function of visibility. This yielded Eq. 3.6, which is the equation that is used in converting transmissometer values to visibility. This equation will be called the transmissometer visibility in this section.

3.1.2 Comparison with Koschmieder Visibility

Equation 3.6 yields a somewhat different relation between visibility and transmittance than is inherent in the daytime definition of visibility. In the daytime, the visibility is defined as the distance at which a black object of certain size may be seen against the horizon sky. It can be shown that this reduces to the equation

$$\epsilon = T^v \quad (3.7)$$

when these ideal conditions are maintained. In Eq. 3.7, ϵ is the human contrast threshold, T is transmissivity, and V is visibility. This is another form of Koschmieder's law (Douglas & Booker Secn 4.1.2). The WMO recommends a threshold of .05. This is the relation used currently in scatter meters. Based on historic data, transmissometers use Eq. 3.7 with a ϵ threshold value of .055.

The day (Koschmieder) and night (transmissometer) visibilities, as defined by Eq. 3.7 and 3.6, are compared in Figures 8 and 9. Figure 8 shows the visibility values as a function of the extinction coefficient (σ in Eq. 3.3). Figure 9 shows the night visibility as a function of day visibility. In Fig. 8, for a given value of extinction coefficient, the day and night visibility values may be quite different. This implies that the value of visibility makes an abrupt change at dusk, even if there is no change in the atmosphere. This is an artifact of the current approach to the definition of visibility; rather than being a term which is a well defined measure of the atmosphere, it is a term which attempts to predict human response. At dusk, as the available targets change, and the human response changes, the visibility determination changes.

3.1.3 Common Usage of the Visibility Equations

Most users appear consistent in using the Koschmieder equation during the day. During the day, transmissometers define visibility in terms of transmissivity using Eq. 3.7, the Koschmieder equation, and a threshold of .055.

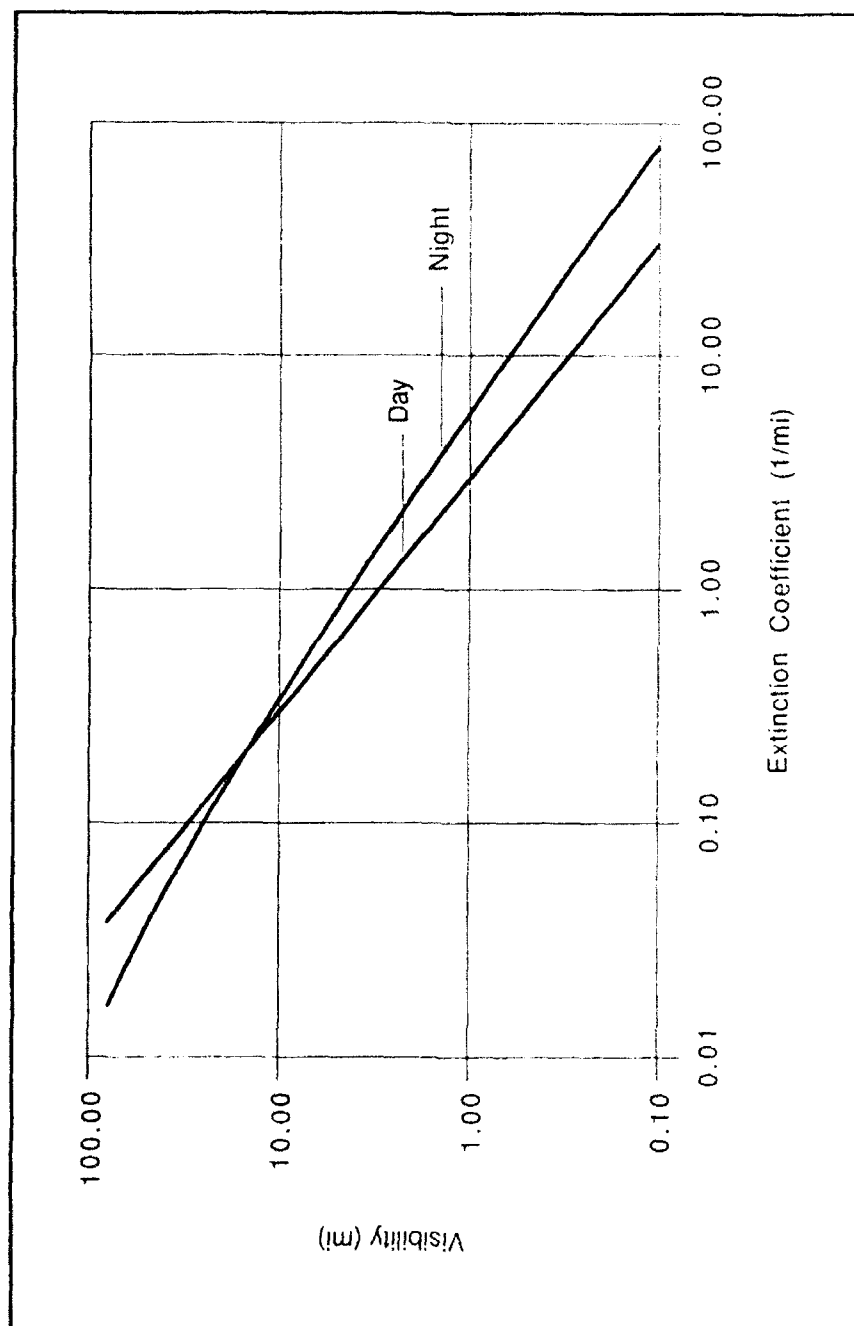


Fig. 8 Koschmieder Visibility (Eqn. 3.7) and Transmissometer Night Visibility (Eqn. 3.6) as a Function of Extinction Coefficient

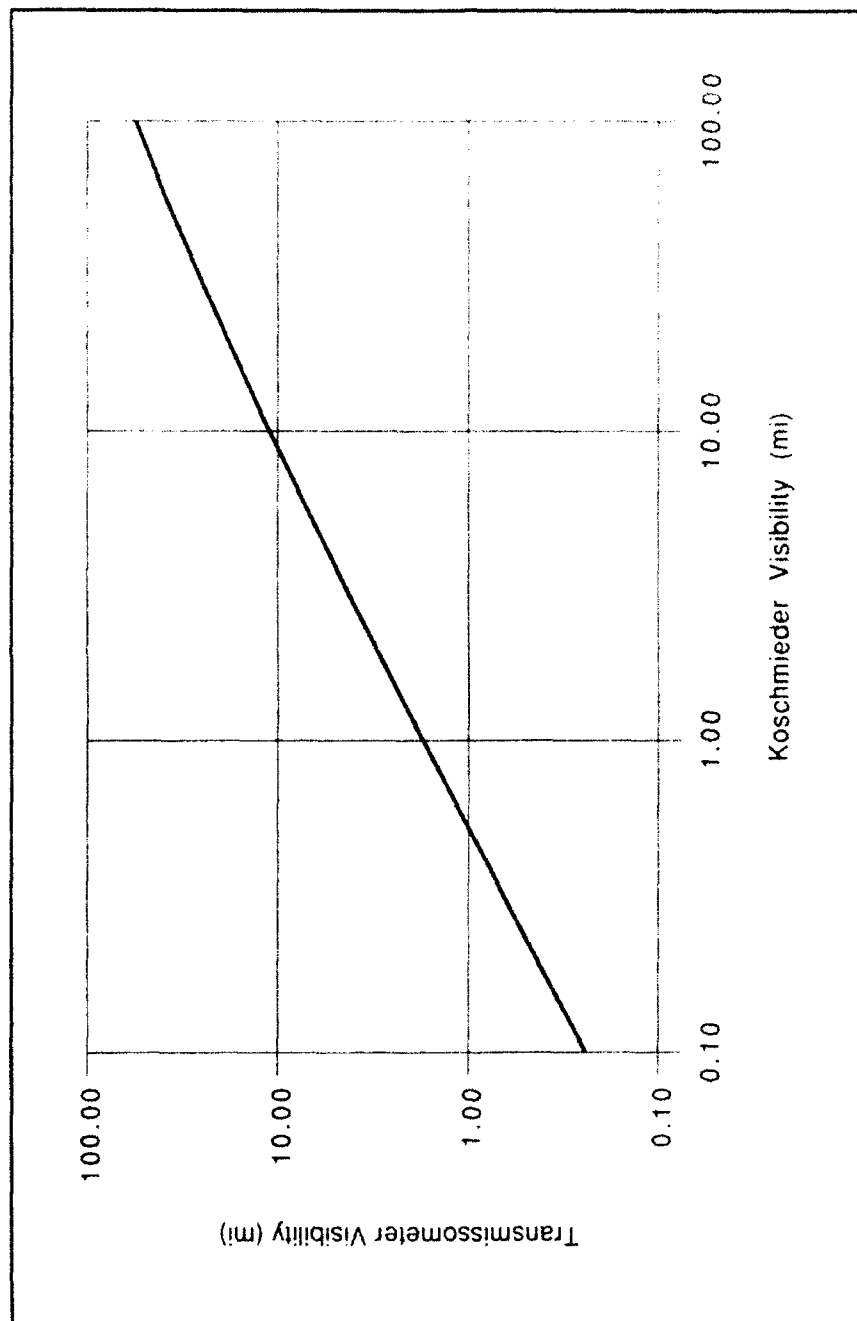


Fig. 9 Transmissometer Night Visibility as a Function of Koschmieder Visibility

Scatter meters use a threshold of .05. The HSI daytime algorithms are also consistent with this definition and a threshold of .05.

At night, even though Allard's law is a defining equation, both Koschmieder visibility equation (Eq. 3.7) and transmissometer visibility equation (Eq. 3.6) are used, as shown in Fig. 10. At night, transmissometers use Eq. 3.6 with a threshold of .084 (mi). The Europeans use Eq. 3.7 and a threshold of .05 at night. Even though the transmissometer output is apparently used only in low visibility conditions, the original tests indicate Eq. 3.6 should also be a reasonable relation to use in clearer air.

Day Visibility	
$\epsilon = T^x$	Koschmieder
$\epsilon = .05$	WMO, Scatter Meters
$\epsilon = .055$	Transmissometers
Night Visibility	
$S = IT^x / V^2$	Allard
$S = IT^x / V$	Transmissometers
$\epsilon = T^x$	European; scatter meters

Fig. 10 Visibility Equation Usage

The weather reports use mostly visually determined values, which are related to the state of the atmosphere, but are certainly not a tight measure of the state of the atmosphere. Under ideal conditions, the psychophysically defined visibility may be theoretically related to the state of the atmosphere. In practice, however, the human often uses targets that are not ideal. If a non-ideal target at a given range is just visible, then that range is defined as the visual range for that target. That visual range as discussed by Douglas & Booker, p. 2-17, is not the same as the visibility.

The level of the background luminance has a strong impact on the ability of a human to see a given light. However the definition of night visibility may be considered to include the stipulation that the light be seen against an essentially black background.

The requirement for black background is not stated explicitly, however Eq. 3.4 and 3.6 are only valid if the background is essentially black. Since this is the normal defining equation, and is also used in applying transmissometer data, it may be considered part of the normal definition.

Douglas and Booker (p. 4-17) discuss the implications of a non-black background in greater detail. In some visual problems, such as runway approach lights, the background is less than 1% of the source. In others, such as with taxiway lights, the background can be significant. It would be feasible with the HSI to correct Eq. 3.6 for the background that obtains at the time of measurement (Douglas & Booker p. 4-17), in order to predict how a human might see 25 candle lights against this particular background.

We propose that the HSI compute the Koschmieder visibility (Eq. 3.7 with a threshold of .05) as the best measure of the state of the atmosphere. In addition, the night transmissometer visibility definition (Eq. 3.6 with a threshold of .084 (mi)) could be used to provide an optional output.

Considering the multiplicity of defining expressions and terms, as noted in the preceding paragraphs, it should be noted that the terms Runway Visibility Value (RVV), Runway Visual Range (RVR), and Meteorological Optical Range (MOR) are other parameters closely related to visibility. A full discussion of these concepts is beyond the scope of this report. A variety of definitions, including psychophysical definitions, are given in Douglas and Booker (1977) and the Federal Meteorological Handbook No. 1 (1988).

3.2 Measuring the Optical Attenuation at Night

The above defining equations relate the visibility to the transmissivity of the atmosphere. This transmissivity may be determined with the HSI using either of two main approaches: basing the computations on absolute measurements, and basing them on relative measurements. Gordon (1989) suggests using measurements of the relative illuminance (apparent) of lights of equal intensity (which is an inherent parameter). Theoretically, it should be feasible to determine the extinction from any set of lights of known inherent relative output. This section discusses first the absolute approach, then the relative approach.

The equations will differ somewhat depending on whether the targets are sub-pixel in size, or larger. If the targets are larger than a pixel, then they may be treated as an extended source, and one uses the measured absolute or relative luminance. If the targets are sub-pixel, they act as a point source. In this case the luminance is undefined and one uses the intensity. Section 3 develops the equations for the extended source.

Note that in this section either the term radiance or luminance could be used. These terms are not equivalent,

however the beam transmittance may be determined from either parameter.

3.2.1 Absolute Measurement Approach

With an extended source, the absolute approach to determining transmissivity is theoretically quite simple. The apparent luminance ${}_iL_r$ of a light at known distance is measured. If the inherent luminance ${}_iL_o$ is known (or derived from clear night measurements), then the beam transmittance may be found from

$$T_r = {}_iL_r / {}_iL_o \quad (3.8)$$

The transmissivity may be derived from the measured luminance by

$$T = T_r^{1/r} = ({}_iL_r / {}_iL_o)^{1/r} \quad (3.9)$$

The Koschmieder visibility equation 3.7 may be expressed as

$$V = \ln \epsilon / \ln T \quad (3.10)$$

Substituting Eq. 3.9 for T , the equation for determining visibility given the absolute luminance values for a target becomes:

$$\frac{V}{r} = \ln \epsilon / \ln ({}_iL_r / {}_iL_o) \quad (3.11)$$

To determine night transmissometer visibility from the absolute measurements, one may use Eq. 3.6, which gives the night transmissometer visibility as a function of the transmissivity. The transmissivity is derived from the measured values using Eq. 3.9. Once this transmissivity is determined, the night transmissometer visibility is determined iteratively from Eq. 3.6.

It should be noted that the night visibility is defined only in terms of point sources (Eq. 3.6 implies a point source). It might seem odd to measure it using extended sources. The reason this is possible is that the transmittance may be determined using either point sources or extended sources. Equation 3.6 then gives an approximate indication of how far a human could see a point source, given an atmosphere with the given transmissivity. (The distance over which a human could see the extended source is not the same as the night transmissometer visibility defined by Eq. 3.6.)

Whereas the absolute approach is theoretically quite convenient, it requires a very stable system, and/or a means of correcting for system absolute response changes. For this reason, it may be preferable to use a visibility determination which does not depend on stability of the sensor over long periods.

3.2.2 Relative Measurement Approach

In this section, we derive the equations which could be used to derive visibility from relative measurements. As in Section 3.2.1, we will assume extended sources; the changes to point sources are given in Section 3.2.3.

Consider a set of sources with known relative inherent illuminance. We will use "L" for absolute illuminance and "N" for relative illuminance. Then source "i" has an absolute inherent illuminance given by

$${}_iL_o = C_1 {}_iN_o \quad (3.12)$$

where C_1 is an unknown constant that is the same for all of the sources. We are able to measure the relative apparent illuminance given by

$${}_iN_r = C_2 {}_iL_r \quad (3.13)$$

where C_2 is an unknown constant that may vary from image to image, as the camera absolute response changes. The apparent illuminance is related to the inherent illuminance by

$${}_iL_r = T^r {}_iL_o \quad (3.14)$$

and therefore the apparent relative illuminance is related to the inherent relative illuminance by

$${}_iN_r = C_2 {}_iL_r = C_2 (T^r {}_iL_o) = C_1 C_2 T^r {}_iN_o \quad (3.15)$$

If one measures the apparent relative illuminance of two sources, with known inherent relative illuminance, one may ratio them to derive the transmissivity, as follows. First, the ratio of the measured relative values is given by

$$\frac{{}_1N_r}{{}_2N_r} = \frac{C_1 C_2 T^{r_1} {}_1N_o}{C_1 C_2 T^{r_2} {}_2N_o} = T^{(r_1 - r_2)} \frac{{}_1N_o}{{}_2N_o} \quad (3.16)$$

Where both targets are from the same image so that C_2 is constant. Taking the logs of both sides yields

$$\ln \left(\frac{{}_1N_r}{{}_2N_r} \right) = (r_1 - r_2) \ln T + \ln \frac{{}_1N_o}{{}_2N_o} \quad (3.17)$$

from which

$$\begin{aligned} \ln T &= \frac{1}{(r_1 - r_2)} \ln \left(\frac{{}_1N_r}{{}_2N_r} \right) - \ln \frac{{}_1N_o}{{}_2N_o} \\ &= \frac{1}{(r_1 - r_2)} \ln \left(\frac{{}_1N_r}{{}_2N_r} \frac{{}_2N_o}{{}_1N_o} \right) \end{aligned} \quad (3.18)$$

Eq. 3.18 may be substituted directly into the equation for Koschmieder visibility, as expressed in Eq. 3.10. This yields an equation for deriving visibility from relative luminance values:

$$V = (r_1 - r_2) \ln \epsilon / \ln \left(\frac{{}_1N_r}{{}_2N_r} \frac{{}_2N_o}{{}_1N_o} \right) \quad (3.19)$$

For night transmissometer visibility, we derive the transmissivity from Eq. 3.18

$$T = \left[\frac{{}_1N_r}{{}_2N_r} \frac{{}_2N_o}{{}_1N_o} \right]^{1/(r_1 - r_2)} \quad (3.20)$$

and then use Eq. 3.6 to iteratively determine the night visibility. As discussed in the previous section, this is the night visibility of point sources, even though it has been derived indirectly by using transmissivity determined from measurements of extended sources.

3.2.3 Summary of the Visibility Equations

As shown in Fig. 11, there are several choices for defining equations to use with the night WSI. First, there is the Koschmieder's law, used during daylight and also used in many cases at night. Next is Allard's law, from which the night transmissometer visibility definition arises. We recommend using the Koschmieder visibility with the HSI, with the night transmissometer visibility as an option to be added at a later time.

On the right side of Fig. 11 are shown the methods of using the HSI to determine the transmissivity which is input to those defining equations on the left half of the figure. The top equation is that used with the HSI during

the day, and is based on the measured contrast. At night, the transmissivity may be determined from either the absolute or relative radiance of lights, as discussed in sections 3.2.1 and 3.2.2, yielding the remaining equations shown in the figure. We feel that the relative approach should be the most accurate determination (due to camera long-term drift), but feel both approaches should be tested. Thus the recommended equations are Eq. 3.19 for the primary equation, and Eq. 3.11 as the alternative test equation.

3.2.4 Conversion to Point Sources

If a given source is smaller than a pixel, then it is effectively a point source. In this case, the luminance of the source is undefined, and the loss of flux is measured in terms of illuminance. The beam transmittance is unchanged, but whereas the loss of luminance is given by Eq. 3.8, the loss of illuminance is given by Eq. 3.2.

One can show that the equations given in Section 3.2 may be converted from extended to point sources by using the apparent illuminance, ${}_1E_r$, in place of the apparent luminance ${}_1N_r$, and by using ${}_1I/r^2$ in place of the inherent luminance ${}_1N_o$. In the above, the intensity is denoted ${}_1I$ rather than ${}_1L_o$, since intensity is by definition an inherent property. Thus, Eq. 3.19 becomes

$$V = (r_1 - r_2) \ln \epsilon / \ln \left[\frac{{}_1E_r}{{}_2E_r} \frac{{}_2I}{{}_1I} \frac{r_1^2}{r_2^2} \right] \quad (3.21)$$

Here E and I should be understood to be relative values of illuminance and intensity and Eq. 3.11 becomes

$$V = r \ln \epsilon / \ln \left[\frac{{}_1E_r}{{}_2E_r} \frac{r^2}{I} \right] \quad (3.22)$$

In practice, if the range to a target will not be changing, it is probably most convenient to use equations analogous to Eq. 3.19 and 3.11 where the apparent property is the apparent illuminance, and the inherent property is the illuminance that would be observed at the target range given zero attenuation. In this way, the system can be programmed with the same equations, whether the sources are point or extended, as long as care is taken in understanding the appropriate inherent property to input.

3.3 Hardware Adaptations for Visibility at Night

In order to determine visibility at night, it was necessary to have a system with sufficient sensitivity for imaging lights of opportunity at night. As discussed in Johnson *et al* (1990), initial tests with an intensified CID system did not yield adequate stability and image quality.

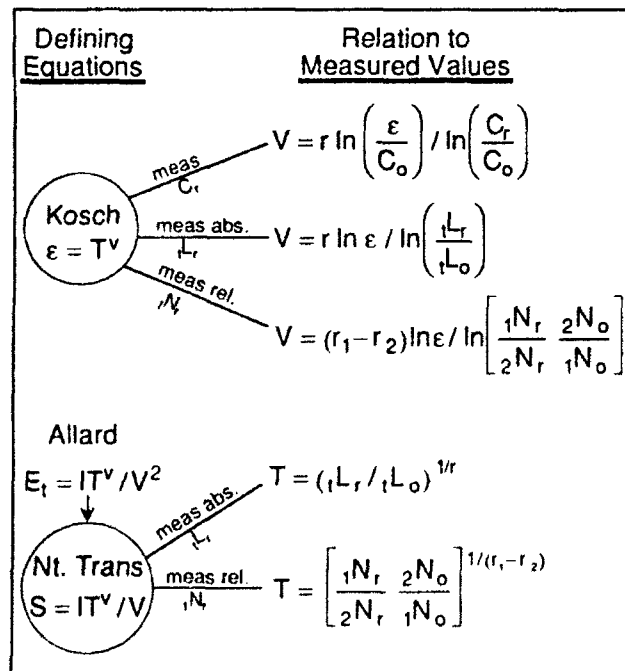


Fig. 11 Defining Equation Relations for HSI Visibility

It was decided to utilize the injection inhibit capability of the CID cameras, in which the signal is allowed to accumulate for multiple frame periods before reading out the accumulated signal (before injecting the electrons into the substrate for readout). This necessitated three changes: changing the camera usage, changing to a new imaging board, and adding an interface circuit.

3.3.1 CID Injection Inhibit

The following description of the CID injection inhibit is extracted from Johnson, *et al*, (1990).

The sensor sub-system used in the HSI is the CID 2710 which incorporates CIDTEC's exclusive Charge Injection Device (CID) sensor into a high-quality, solid state, monochrome RS-170 camera. (Ref. Vol. II)

"The Charge Injection Device is an X-Y addressable image sensor organized so that photon-generated charge can be read at each sensing site (pixel) through local charge transfer. Injection into the underlying substrate is used to clear each pixel of signal charge and start a new signal integration period (television frame time). These images are fabricated in an epitaxial layer; the epitaxial junction is reverse biased and used as a common collector to remove the injected charge from the device. The consequences of this organization are numerous. Since charge is sensed locally, there are no paths along which optical overloads or defects (black or white faults) can propagate. Charge transfer losses are not cumulative. Pixels can be contiguous, leading to high modulation transfer function and high quantum efficiency. The sensor has inherently low dark current; the depletion region of each pixel is smaller than the photo sensitive region and inversion charge can be used to quench surface leakage current. Read-out can be non-destructive allowing on-chip signal processing, and the X-Y addressable array can be random accessed." (Grafinger & Michon)

The HSI system takes advantage of the inherent characteristics of the CID 2710 camera system to address several low light level measurement scenarios without the need for external image intensification. This is accomplished by implementing the Inject Inhibit function available in the standard camera configuration. In this mode, normal destructive readout is interrupted by the Inject Inhibit function which permits the imager to integrate for longer than one frame time. The 2710 continues to integrate as long as the Inject Inhibit function is engaged, facilitating user controlled time exposure. Several mock-up circuit boards were built by MPL to enable the selection of integration intervals ranging between 2 and 200 frames. At standard video rates of 30

frames per second, these integration intervals represent roughly 60 milliseconds upward to 6 seconds.

3.3.2 The VS-100 Image Board

Under integration, the CID camera outputs a signal which remains in RS170 format, however during the integration interval, the output frames on the RS170 signal have 0 analog signal, i.e. are black. Figure 12 shows a simplified rendition of the RS170 signal at vertical frame rate. At 0 integration, i.e. normal video rate, the CID outputs each field separated by vertical sync information, with two fields creating a full frame. (Each field consists of the output from either even or odd scan lines, with horizontal sync information between lines, ref Varah and Sprink, 1991.) With integration set to 1, the camera integrates during an extra frame, during which time the active video output is 0. This is followed by a frame with the integrated video signal read out. Similarly, as shown in Fig. 12, at higher integration settings, the video output is 0 during integration, followed by a read-out frame.

The signal is read by the control system through an imaging board, which performs the following on-board functions: A/D conversion, frame memory, image processing, and D/A for display on the monitor. The daytime HSI and WSI both use an Imaging Technology FG-100 board. For night operation with the injection inhibit function, it was necessary to change to the VS-100 board. The primary new feature of this board used in this application is the external trigger. That is, this board allows use of an external trigger for frame grab, so that the readout frame could be grabbed, rather than one of the black frames output during integration.

3.3.3 The Integration Control Circuit

In order to fully synchronize the VS-100 board with the camera injection inhibit, it was necessary to design and build an integration control circuit. This circuit is documented in Varah and Sprink (1991).

The control interface allows control of the integration period either through computer, or manually via thumb wheels. The control circuit, synced by the vertical sync from the camera, sends a signal to the camera to start integration. At the same time, it begins counting integration periods. On completion of the desired integration interval, it sends a signal to the frame board to grab the next output frame, and sends a signal to the camera to stop integration. The above is a conceptual overview; in practice, the control is considerably complicated by the need for appropriate delays for coordinating the camera and frame board.

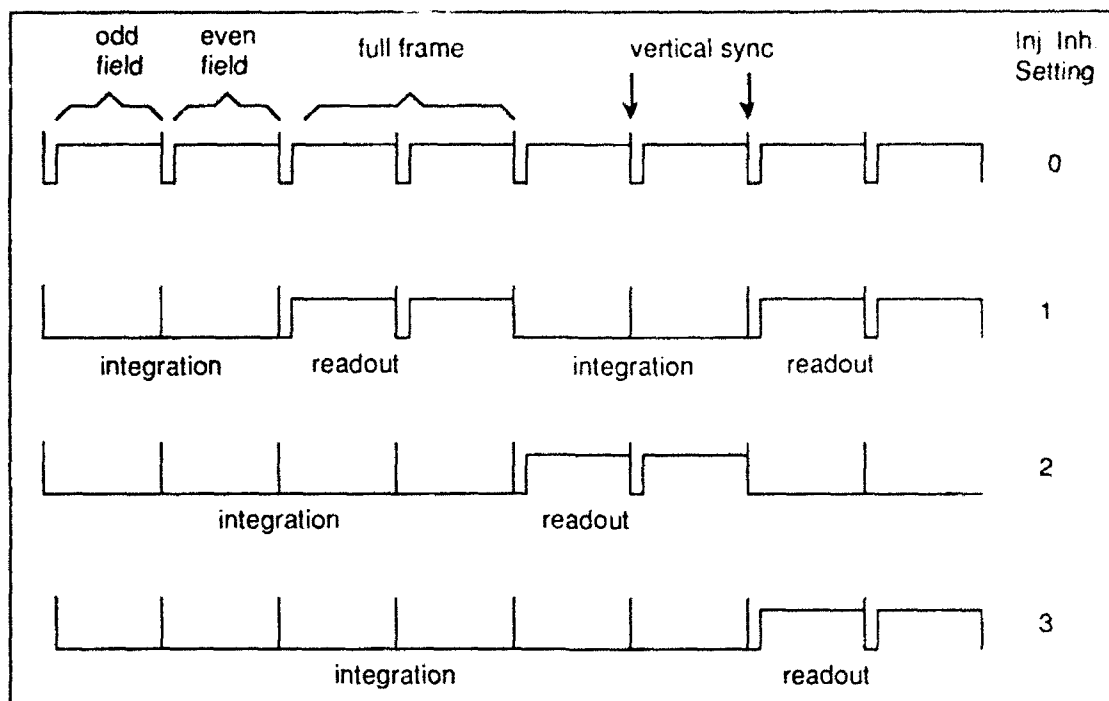


Fig. 12 Conceptual illustration of output RS170 Video Signal
(Vertical frame rate) at various injection inhibit settings

3.3.4 The Auto-iris Inhibit

Normally the auto-iris reads the output video signal, and adjusts the aperture opening to keep the signal at some preset level, nominally mid-scale. There were two concerns with the use of the auto iris at night. First, if the camera integrated long enough for the signal to become reasonably bright, the iris might begin to close in response. This would be counter-productive; it makes no sense to use integration for increased signal, then decrease the signal with an aperture. Secondly, depending on the integration period used with the iris, there might be unpredictable response to the changing video output during integration, as the output changes from black during integration to grey during readout (as shown in Fig 12).

In order to defeat these problems, it was decided to control the auto iris such that any time injection inhibit is used, the auto iris is disabled and forced fully open. When an injection inhibit setting of 0, or video rate is used, the auto iris is enabled.

All of the above hardware changes have been built and tested. They perform normally, and are considered operational at this time.

3.4 Software Adaptations for Visibility at Night

There were very significant changes to the HSI/WSI software during the last year. As discussed in section 3.4.1, software to enable night data acquisition was written. Section 3.4.2 discusses the changes to the daytime code, for compatibility with the new VS-100 imaging board. Additional changes to the daytime code, to enhance its capabilities, are discussed in Section 4, which discusses refinements to the HSI daytime capabilities.

3.4.1 Night HSI Programs

Three programs were written for handling data acquisition with integration. The primary program for night data acquisition is Program GETNITE. This program is designed to run unattended, to let the user grab night imagery and store the images on Exabyte tape. The user may enter start time and stop time, and acquire images at a variety of integration levels automatically.

Program INTGR8 is a utility designed for use in calibration and other camera tests. This program allows the user to enter the integration level either via keyboard or manually, and acquire and save imagery. The integration level may be varied during the program.

Finally, Program VSUTIL is a general utility program for accessing the VS100 board. It was quite preliminary, however it may still be used for accessing the data stored on tape, when a machine with a VS100 board in place is used. This is not normally used in-house, as imagery saved with any of the above programs may be accessed on any of the in-house computers with FG-100 boards.

3.4.2 Adaptation of the Day HSI/WSI programs for VS-100

Changing from the FG100 image board to the VS-100 board, to enable using injection inhibit for on-board integration with the CID, had one unfortunate result: the software had to be changed, even for daytime use, because the VS-100 board is not downwardly compatible with the FG-100 board. As a result, all of the daytime code, for both WSI and HSI, had to be changed. These programs are listed below.

Primary Programs

- Setupvis - Creates azimuth selection file, allows user to change input parameters (range, threshold and inherent contrast).
- Vistex15 - Automated visibility determination program.
- Wsitex - Cloud cover determination program.
- Fixhome - Fine tunes home position.
- AV5 - Program is now called Snglvis. Computes visibility for a range of inherent contrasts.
- Seevis - Displays image disk file to RGB screen.
- Savimg - Allows user to digitize an image, then save it to disk.
- Savrgb - Allows user to save image currently on RGB screen to disk.
- Viewvis - 8mm data tape created by Vistex 15.

Programs such as Move which move the rotary table to a user selected azimuth and Printvis which prints and translates visibility data files into a spreadsheet format are not affected by the VS100 board.

The changes to the daytime programs to enhance to enhance their capability are discussed in Section 4.

3.5 CID Camera Behavior under Integration

In order to acquire the night data, it was necessary to use the CID camera in integration mode, as discussed in Section 3.3. A series of tests and radiometric calibrations were run on the CID cameras to determine whether this mode of operation introduced any signal peculiarities which must be accounted for in the data handling.

Several in-house cameras were tested, and found to be deficient in a variety of ways, even though they behaved well under normal video mode use. Since the faults appeared to be related to aging, two new cameras were purchased. These were found to behave adequately. This section first describes the behavior of the new sensors, and then discusses the types of faults which occurred in those cameras which had begun to age.

The CID camera is reasonably linear, in the sense that a fractional change in input flux yields a similar fractional change in output signal. Fig. 13 shows the results of a linearity calibration, acquired at normal video rate. The system is quite linear over most of the span, with some decrease in signal relative to the expected signal at the bright end. This is quite typical of the CID sensors. If the sensor is used in the visibility system without correcting for this slight non-linearity, the resulting error is typically 7%, when the horizon radiant signal is about 200. As mentioned earlier, we recommend changing the current HSI algorithms by applying the linearity calibration results to the imagery to correct for the non-linearity.

When the sensor is calibrated using integration, an abnormal feature becomes immediately apparent on many of the cameras, including one of the two new ones. The alternate field lines have slightly different magnitude; that is, the odd field and even field have slightly different signals (ref Fig. 12). Whereas it is part of our normal procedure to adjust the alternate field lines at normal video rate in the electronic calibration, there is not a way to adjust this under integration. As an example, the new camera with this problem had a standard deviation in the signal over a 20 x 20 pixel square of 2 counts in video mode, and about 10 counts at integration level 1.

As shown in Fig. 12, the output signal is nominally zero during the integration period. With those sensors showing the alternate field offset, there is a non-zero signal for one of the fields even during the integration period. For this reason, we would recommend further evaluation of potential ways to correct this alternate field problem prior to purchase of any additional units. It may be preferable at this point to convert to a CCD sensor, if one with better operating characteristics is available at a similar price.

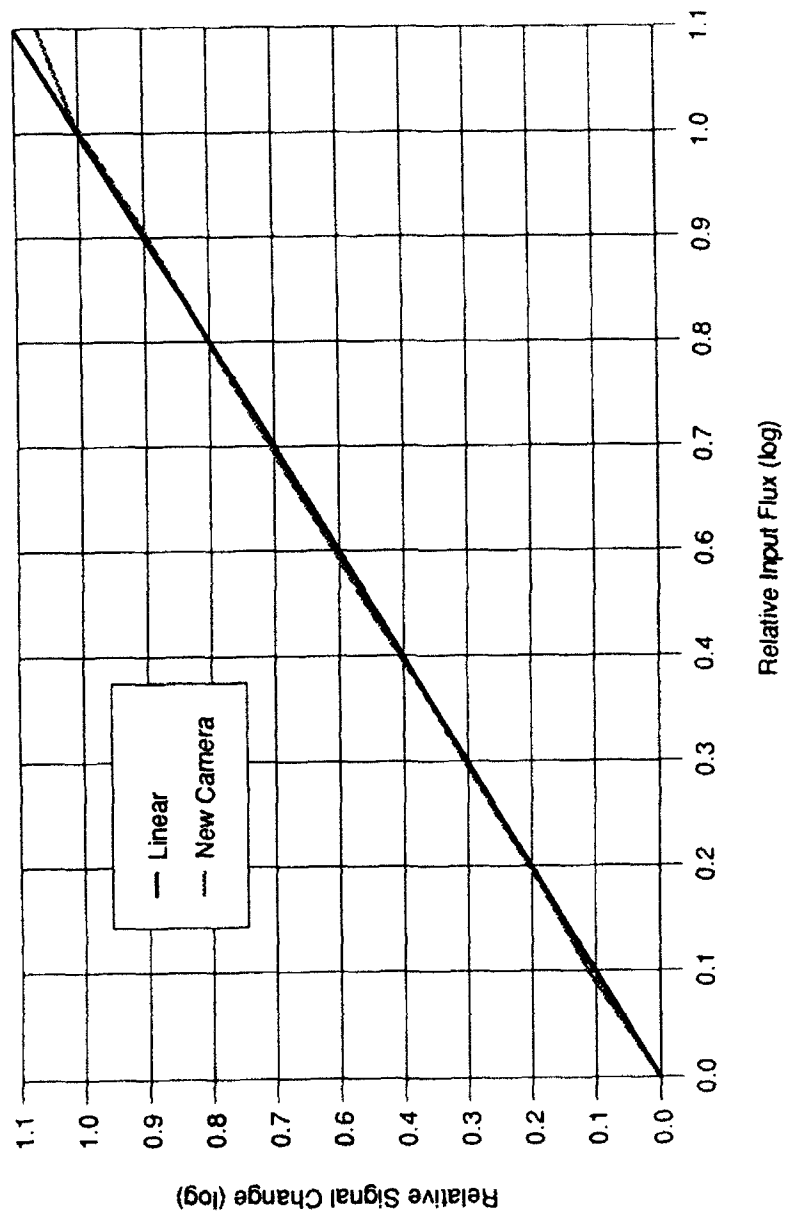


Fig. 13 Results of the Linearity Calibration, showing the slight non-linearity of the CID Sensor at 0 integration

Results from a sample calibration of signal vs. integration period are illustrated in Fig. 14. The pixels continue to receive flux during the readout interval, as well as during the integration interval, so the expected signal should be proportional to $(I + 1)$, where I is the integration interval. In Fig. 14, the straight line represents this expected relationship. The measured response is quite close to this expected response. The lower curve in Fig. 14 will be discussed later in this section.

Measurements similar to those shown in Fig. 14 were also acquired for a variety of other signal levels and integration periods. It was determined that whereas this camera is well-behaved out to an integration of 10 periods, the signal is non-linear beyond an integration level of 20 periods, even when the signal is low enough to be well onscale. Beyond 20, the signal becomes quite non-linear, with an output lower than expected based on the $(I + 1)$ relationship.

Thus the new CID sensors were reasonably linear in terms of signal vs. input flux, and quite linear in terms of signal vs. integration period out to 10 periods integration. The CID performance in other respects was quite adequate, except that some new sensors apparently have a field offset in integration mode which degrades the quality of the measurements.

The response of the CID sensors to aging is also a serious concern with respect to their use under integration. We had in-house several sensors of varying ages, which were still quite good for normal full video rate usage. That is, the dark levels were reasonably low, standard deviations low, and other features such as ramping and field offset low. However, under integration, none of these older sensors (same model, longer usage) performed adequately. One camera had full dark levels which became quite high under integration. Another had a severe field offset problem.

The most common problem with these older CID sensors was that the behavior with integration was no longer linear. The lower curve in Fig. 14 illustrates the rolloff feature vs. integration period, which was common to the older cameras. Not only was this rolloff quite camera dependent, but it was scene dependent. The example given was acquired with a uniform image, i.e. one brightness level over the full array. The rolloff was much more extreme when only one portion of the array was illuminated. Thus the calibration becomes both scene and integration level dependent in the older sensors.

We do not know what aging rate is critical for the sensors. We feel that the problem may be due to recom-

bination of the electron-hole pairs at the sites of crystal defects, and that a measure of the background dark level may be in reasonable indication of this aging process in the crystal. However this is surmise only at this point.

It is fair to say that the CID sensors are quite effective for daytime visibility, and are adequate for night tests required to further develop the concept of determining visibility at night. However these sensors are not optimal over the long term for night visibility acquisition, due to their unfavorable response under integration after aging. Slow scan CCD sensors have more than adequate sensitivity for both night and day visibility applications, at a higher cost. A high priority should be evaluation of the relative cost and merits of the variety of solid state sensors currently available for this task.

3.6 Sample Night Visibility Computations

To provide a sample computation of the techniques discussed in the previous sections, we acquired data during the daylight and evening hours on a clear day and a foggy day. First, the sample daytime images extracted for study were used to derive daytime visibility in the normal manner. The results were about 26 miles on the clear day, and 2 miles on the foggy day, as shown in Table 1.

Table 1
Day Visibility Sample Values

Date	Time	Azimuth	Visibility
16 Jan	234224	80	28 mi
16 Jan	235651	110	25 mi
23 Jan	001224	80	< 2.6 mi
23 Jan	002651	110	2.0 mi

In order to evaluate the night data, we first had to estimate the inherent signal, i.e. the signal corresponding to 100% transmittance. To do this, we assumed that at night on the 16th the visibility was still about 26 miles and used this data to determine the inherent signal from selected lights. Then using this approximate inherent value, we computed the visibility for 23 Jan at night, using the measured night signals.

We were able to find 4 targets which were onscale both nights at the same integration period, at azimuth 80. At azimuth 110, there were no targets onscale both nights with the same integration period, but the use of different integration periods allowed selection of two targets with onscale data on both nights.

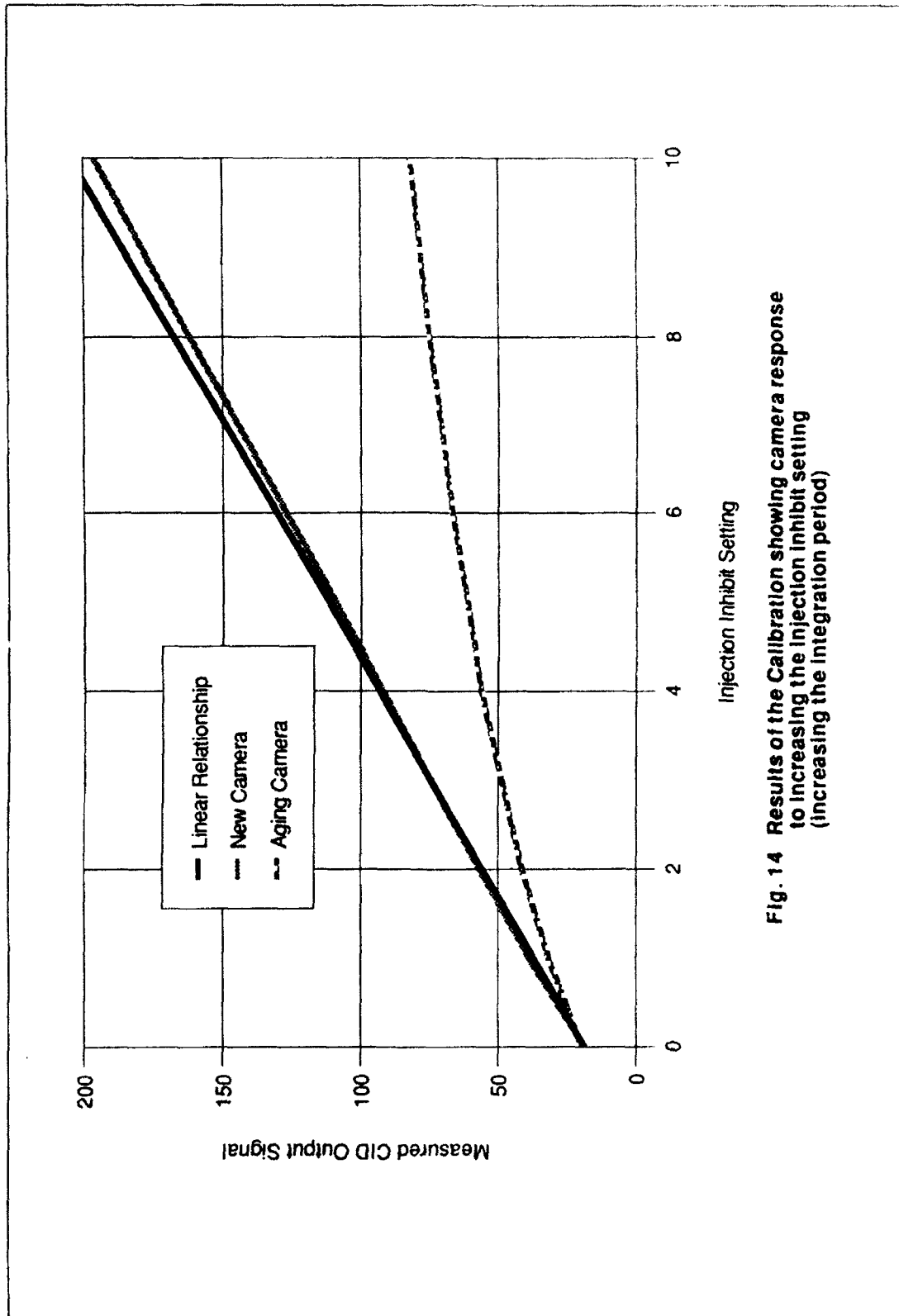


Fig. 14 Results of the Calibration showing camera response to increasing the Injection Inhibit Setting (increasing the integration period)

The computation of the inherent signal is shown in Table 2. In Table 2, data have been extracted from the clear night images. The background signal, a combination of path radiance and sensor dark level, was extracted a few pixels below the light, and the signal corrected for the background is computed. Given the range to the target, the approximate transmittance may be estimated, assuming a visibility of 26 miles (the visibility measured earlier during the day). From this computed transmittance and the background corrected signal, we may compute the signal which should occur if the beam transmittance were 100%. This is labeled the "pseudo inherent signal". This label reflects the fact that since many of these lights may be point sources, the pseudo inherent signal does not refer to the signal at zero range;

rather it refers in this case to the signal at the given range which should occur if the transmittance were 100%.

Once a pseudo inherent signal is computed for each target, the data from other nights may be used to estimate the visibility. This procedure is illustrated in Table 3 using the foggy night images. In this table, the first signal shown is the pseudo inherent signal from Table 2. Next is the raw signal and adjacent background, which is subtracted to yield the corrected signal. At the 110 azimuth, the corrected signal also reflects an adjustment for the integration period of 7, to correct it to the signal appropriate for an integration period of 4. The visibility is then computed directly from Eq. 3.11, the derived visibility equation using the absolute approach.

Table 2
Computation of Inherent Signal From Clear Night Data (16 Jan)

Date	Tgt #	Raw Sig	Bkgnd	Corr Sig	Range (mi)	Est Trans.	Pseudo Inh. Sig.
Azimuth 80, Int level 4, Time 040601							
16 Jan	1	174	36	138	1.2	.87	159
16 Jan	2	107	29	78	1.1	.88	89
16 Jan	3	95	28	67	1.1	.88	76
16 Jan	4	217	30	187	1.1	.88	212
Azimuth 110, Int level 4, Time 035019							
16 Jan	5	112	28	84	2.8	.72	117
16 Jan	6	182	20	162	2.8	.72	225

Table 3
Computation of Foggy Night Visibility (23 Jan) Using Absolute Equation

Date	Tgt #	Pseudo Inh. Sig.	Raw Signal	Bkgnd	Corr Sig	Vis (mi)
Azimuth 80, Int level 4, Time 040601						
23 Jan	1	159	71	28	43	2.8
23 Jan	2	89	52	25	27	2.8
23 Jan	3	76	49	25	24	2.9
23 Jan	4	212	39	26	13	1.2
Azimuth 110, Int level 4, Time 042218						
23 Jan	5	117	53	28	15.6*	4.2
23 Jan	6	225	50	30	12.5*	2.9

*Corrected for both background signal and Integration 7 vs Integration 4 calibration

In Table 3, most of the values are reasonably consistent indicating a visibility of about 3 miles. This is consistent with the daytime visibility of 2 miles measured earlier in the day. Those discrepancies that occur may have been caused by the use of some lights with varying output. In actual practice, it would be necessary to build a library of target lights with reasonably steady output. For an initial sample, these results are reasonably encouraging.

The relative approach given by Eq. 3.19 may also be illustrated with these data. Two examples are given in Table 4. Here Target 5, which yielded a somewhat inconsistent visibility in Table 3, using the absolute approach, yields a slightly more inconsistent value using the relative approach. Target 6, which yielded a consistent result using the absolute approach in Table 3, also yielded a consistent result using the relative approach in Table 4.

In summary, the equations developed in Section 3.2 yielded reasonable results in this case study. During the day, the visibilities were around 26 miles on 16 January and 2 miles on 23 January. If one assumes that the visibility (Koschmieder visibility) was still about 26 miles at night on 16 January, the computed visibility for 23 January at night was about 3 miles. Given that the aerosol may have in fact changed with the onset of evening, these are quite reasonable results.

To automate this technique would require several steps. Sensitivity studies, to evaluate the relative merits of the absolute and relative technique should be done. In addition, it would be necessary to determine which light sources are most steady, and do a more thorough determination of their inherent characteristics. We feel the night visibility results are sufficiently promising to recommend continued development in this area.

4. DAYTIME HSI/WSI SYSTEM REFINEMENTS

A number of improvements to the daytime capabilities of the HSI/WSI system were evaluated and/or in-

stalled. In this next section, we first review the refinements which have been fully programmed. There is a discussion of an in-depth sensitivity study of the HSI, which revealed a number of areas of potential system improvement. Finally, there is a discussion of a recommended change to the day visibility equations in use in the HSI.

4.1 Changes to the HSI/WSI Programs

In addition to the changes discussed in Section 3.4, to enable using the daytime programs with the VS-100 imaging board, several other changes to the daytime programs were made.

Perhaps the most significant is that the number of allowable targets within a scene was increased to 16. This is important in increasing the accuracy of the determination, for the following reasons. As noted in Shields, et al, (1991), the error in visibility determination due to changes in the inherent contrast of the target with respect to the background can become quite large when the target range becomes short with respect to the visibility, i.e. when V/r becomes high. On the other hand, the error in visibility determination due to errors in measured target or horizon radiance become large when the target range approaches the visibility too closely, i.e. when V/r is too close to 1.

For these reasons, the HSI algorithm has automatic cutoff values for V/r . If V/r for a given target is between 1.15 and 4.0, the visibility determined using that target is given preference in the sorting algorithm which determines the final visibility for a given sector. Thus, on a clear day, the optimum targets may be quite distant, whereas on a hazy day, the optimum targets will be closer to the observer.

By allowing the use of up to 16 targets within a given scene, it becomes possible to have several targets at a wide variety of ranges. Thus it becomes more likely that for a given visibility condition the HSI has targets within the optimal range, and can thus yield a more accurate value.

Table 4
Computation of 23 Jan Visibility Using Relative Equation
Night Visibility using Relative Approach

Point 1	Point 2	r_1	r_2	$1N_r$	$2N_r$	$1N_o$	$2N_o$	Vis (mi)
Tgt. 5	Tgt. 2	2.8	1.1	15.6	27	117	89	6.2
Tgt. 6	Tgt. 2	2.8	1.1	12.5	27	225	89	3.0

The HSI programs have also been changed to allow selection of larger horizon regions of interest (ROI). One of the uncertainties with the HSI is the error caused when there are clouds present in the horizon ROI. By selecting larger ROI's, the user can evaluate the variance within the horizon ROI. We recommend using two horizon ROI's, and adding an automated check which determines if both regions have similar averages and low STD's, as a means of detecting significant cloud contamination.

Several additional program changes were made for user convenience. These include saving a raw image without the ROI's overlaid (in addition to saving the image with ROI's), embedding the target information in an image header, saving the WSI information to disk, and updating the Program SNGLVIS, which allows later evaluation of archived images.

4.2 Sensitivity Study of Daytime Visibility

A sensitivity study was made, to determine the most significant sources of error in the HSI system. This study, Shields, et al, (1991), evaluated the impact of changes in the inherent contrast of the target, measurement errors, and changes in camera sensitivity. The summary and recommendations from this report are extracted below.

4.2.1 Summary of the Sensitivity Study

Two summary plots, containing curves extracted from the earlier sections, have been created: one for $C_0 = .8$, $L_q = 200$, and one for $C_0 = .5$, $L_q = 200$. In these plots, shown in Fig. 15 and 16, the four curves show: the impact of a C_0 change of .1; the impact of a measured target radiance change of 4 (on the 0 to 255 scale); the impact of a measured horizon radiance change of 4; and the impact of system non-linearity for the system at Otis.

All of these uncertainties can cause a certain amount of error. The sensitivity to C_0 uncertainty is very small when the target range is close to the visibility (near $C_T = .05$), and fairly large when the target is closer. Unfortunately however, the measurement uncertainties cause the most error when the target range is close to the visibility. That is, when the C_0 impacts are least, the measurement error impacts are largest.

There are some techniques for improving our C_0 estimates, but in the final analysis the C_0 changes may be most difficult to handle. The measurement uncertainties may in many cases be mitigated by a combination of improved measurements techniques and improved data reduction techniques. As the magnitude and/or impact of measurement uncertainties are improved, it should be possible to chose targets closer to the visual threshold,

which should help mitigate the impact of the C_0 uncertainties.

Another way to look at the system is to consider that the ability to determine visibility from targets ranging near the visibility depends on the ability to accurately determine the difference between signals which are quite close. This requires precision, stability, and accuracy in the measurements acquired by the system. At the other extreme, the ability to determine visibility from targets which are at close range (and which therefore have apparent contrast somewhat close to the inherent contrast) depends on our ability to accurately characterize the C_0 values and their fluctuations.

In the short run, there are obvious ways in which improvements can be made in terms of measurements. These include keeping the horizon radiance near 200, and measuring and applying the non-linearity correction. Other potential improvements such as correcting for chip non-uniformity, to improve measurement accuracy, may or may not be warranted. There are a variety of tests to help us determine questions such as this one.

A significant improvement in the current accuracy should be readily realized as these changes are enacted. In the long run, as solid state sensors improve in stability and noise handling, we should expect significant improvements in the measurement capabilities. These in turn should allow us to make better use of the measurement regimes in which the sensitivity to C_0 changes becomes small.

As an outcome of this study, there are a number of changes and/or tests which should be considered. These fall roughly into two categories. The first category is changes having to do with measurement accuracy, including both improvements to the measurement accuracy, and changes to mitigate the impact of measurement inaccuracy. The second category is changes having to do with the handling of non-ideal measurement conditions, such as non-ideal targets or non-ideal horizon skies. These two types of improvement categories will be discussed below.

4.2.2 Recommended Improvements Relating to Measurement Accuracy

The first and most obvious change recommended is to ensure that the horizon radiance is near 200 counts. Whereas this does not in itself increase the measurement accuracy, it significantly mitigates the effects of measurement inaccuracy. With the MPL unit, the horizon signal is currently near 100; we need to verify that the camera response has not become truncated due to inter-

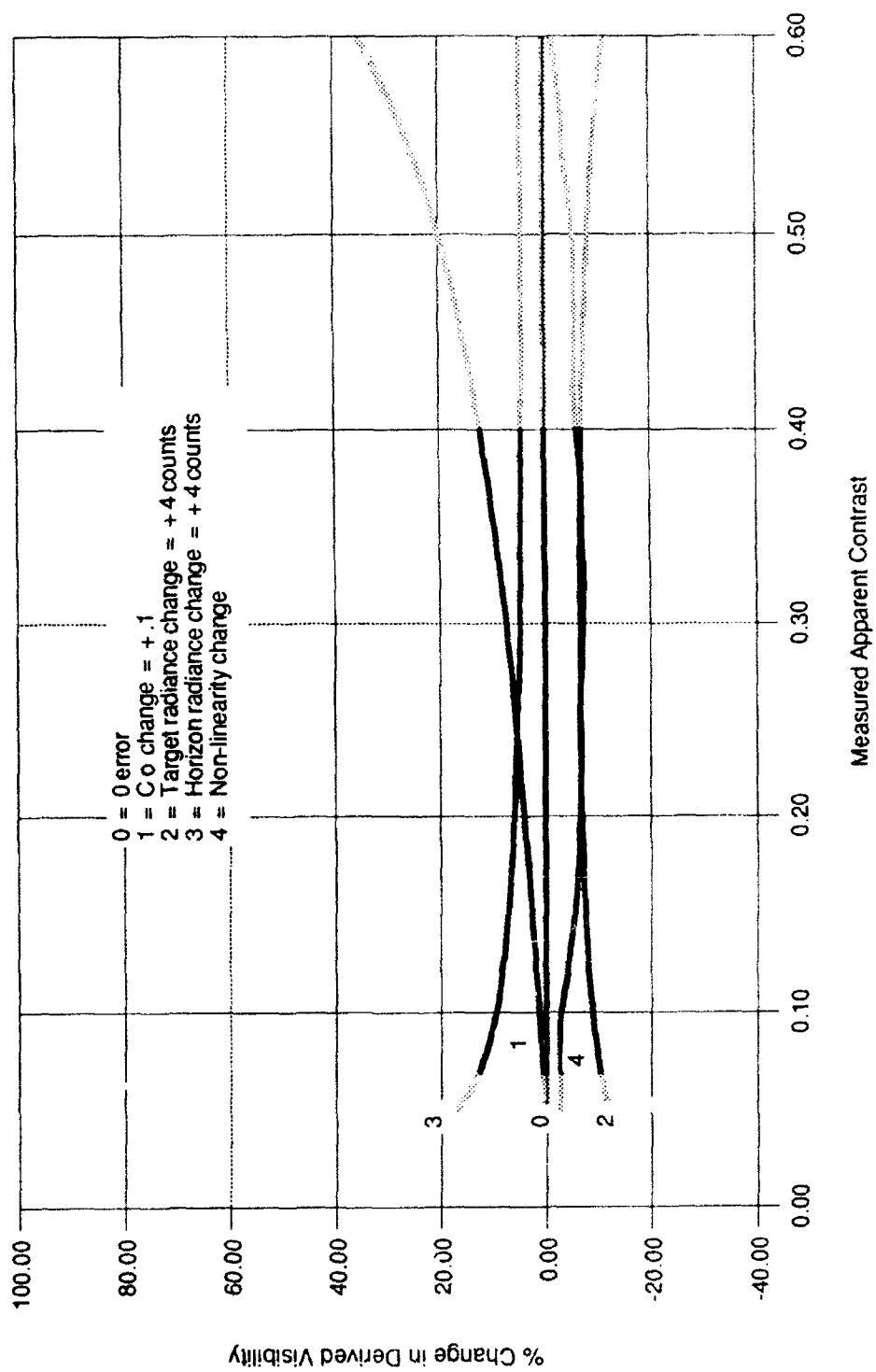


Fig. 15 Error in visibility due to system or input errors, when $C_0 = .8$ and $Lq = 200$

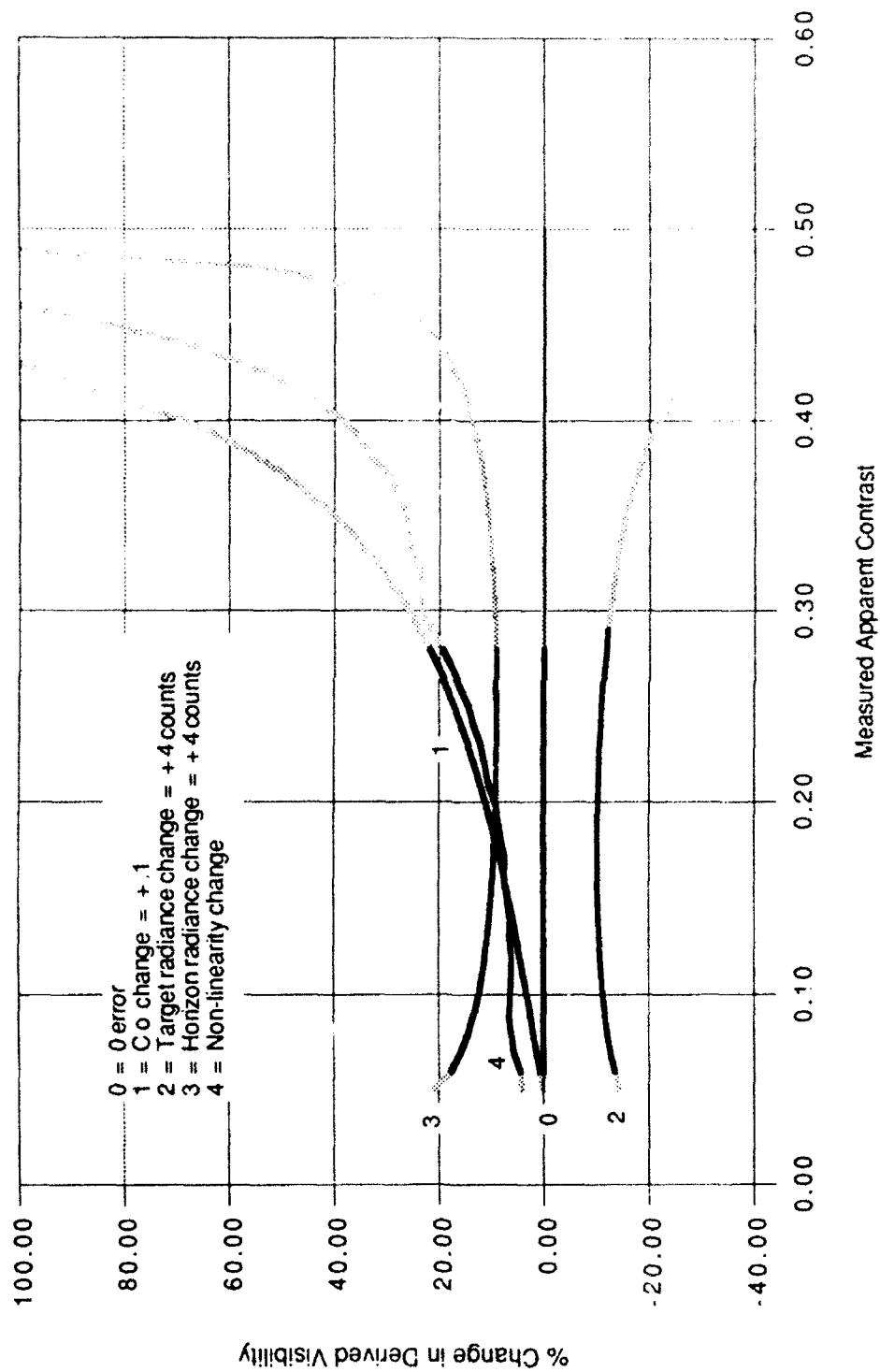


Fig. 16 Error in visibility due to system or input errors, when $C_0 = .5$ and $Lq = 200$

nal problems, and then adjust the auto-iris to yield a horizon brightness near 200. With the Otis unit, we similarly need to determine the current signals which occur for the horizon, and optimize them as necessary.

We need to acquire a new linearity calibration for the MPL unit, to determine how much change, if any, has occurred since the original calibration. It will be somewhat more difficult to acquire a linearity calibration for the Otis unit, but this is certainly something to do when possible. I would propose that we incorporate application of the linearity correction into a test version of the software. We should devise a technique for testing the sensor response in the field. Installation of a light trap, to enable testing of the dark end of the responsivity curve, could help us begin testing the efficacy of this sort of *in-situ* procedure.

Next, there are several tests that involve investigation of the magnitude of existing measurement errors. As discussed earlier, both the horizon and target radiances are impacted by noise, changes in full dark, and chip non-uniformity. Any change in full dark may be treated as part of the sensor responsivity change documented by the linearity calibration, and need not be treated separately for now.

The magnitude of system noise averaged over the horizon and target ROI's may be evaluated by grabbing several images of the same scene in close temporal succession, and comparing the resulting signals averaged over the ROI's. The errors due to chip non-uniformity may be evaluated using the linearity calibration data. If one wants to know the magnitude of non-uniformity for a given target location, one extracts the signal for that target ROI and for the horizon ROI, but using a calibration image of a uniform source. We can then decide if either system noise or chip non-uniformity cause errors large enough to require compensation.

Since the impact of measurement error is worst as V/r approaches the lower limit of 1.15, and the impact of non-ideal C_0 is worst as V/r approaches 4.0, there is benefit in avoiding these limits. Since the optimum range is a function of the visibility, it is important to have enough targets so that there are always several within the optimum range, for all possible visibility values.

Within the limits imposed by the availability of real world targets, an effort should be made to select many targets over a range of target distances. (For those familiar with transmissometers, it may be helpful to note that whereas a transmissometer is reasonably accurate over a range of visibility values determined by its base

length, the HSI is reasonably accurate over a range of visibility values determined by the target ranges. By using very near targets under low visibility conditions, and far targets under high visibility conditions, we are creating an impact similar to adjusting the transmissometer base length.)

Note also that it is very important that the range to these targets be determined accurately, since the error in visibility due to an error in range is directly proportional to the range error. This may involve driving out to the sites, and visually identifying the targets being used.

4.2.3 Recommended Improvements Relating to Non-ideal Conditions

There are several things which can be done to improve the system with regard to non-ideal conditions. First, consider the impact of horizon sky problems. If the measured horizon radiance is not equal to the equilibrium radiance, there is a corresponding error in the visibility. Under clear sky conditions, the near-horizon radiance is expected to decrease away from the equilibrium radiance value as the elevation angle is increased. This occurs due to the decreasing turbidity of the path of sight.

It would be instructive to extract the change in horizon radiance over the range of elevation angle in the HSI field-of-view. This can be done with existing HSI imagery. This would allow us to determine the range of elevation angles which provide a sufficiently accurate determination of the equilibrium radiance (in the absence of clouds).

Similarly, we should investigate the incidence of clouds on the horizon which are bright enough to cause error. We can probably improve our handling of this possibility by using two horizon ROI's, and checking the signal standard deviation in each, as well as the difference in the average signals. If one ROI has a high STD and/or elevated signal, use of the other ROI might avoid the cloud. If both ROI's have high STD's, there is probably little that can be done currently other than alert the user, or potentially not use the visibility for that scene. A test program to investigate these possibilities should be implemented.

Over the longer run, the case of cloud clutter at the horizon might be addressed by the next generation larger field-of-view WSI. If we make determinations using the WSI of where the clouds are, it should be feasible to utilize horizon ROI's which are in the clear areas indicated by the WSI. Similarly, introduction of a red/blue filter changer to the HSI could allow determination of the clear horizon regions for use in visibility determination.

Finally comes the really difficult problem, changes in C_0 . Once we have improved the accuracy of the system in the ways discussed above, we will probably want to tackle determination of C_0 . This is done by using the median visibility determined from the available targets, or an independently determined visibility, then determining what C_0 values for each target will yield that visibility.

It would be very helpful to run curves similar to the ones in Shields, et al, (1991), which determine the sensitivity of the C_0 determination to known errors, so that we can adjust our technique appropriately. (For example, we know intuitively that the targets must be at close range, relative to the visibility, in order for visibility to be sensitive to C_0 , which means targets must be close to back out the C_0 value. But does measurement error then cause undue problems?)

If we are successful with C_0 extraction, a study of the time variation in C_0 would be helpful. The equilibrium radiance is expected to change as a function of the scattering angle with respect to the sun. This gives us a theoretical change in C_0 due to the change in the horizon brightness. If this is dominant over changes due to target brightness, the diurnal changes in C_0 might be reasonably predictable.

4.3 Recommended Change to the HSI Visibility Equation

The HSI uses Eq. 2.2 to determine visibility from the measured apparent contrast of targets with respect to the horizon. At this time, it is recommended that the system be changed to use the equation

$$V = r \ln \epsilon / \ln \left(\frac{C_r}{C_0} \right) \quad (4.1)$$

The current equation provides an estimate that is a compromise between visibility and the human estimate of visibility; this estimate is target dependent. Equation 4.1 would provide visibility determination consistent with defined visibility, and yield a result which is not target dependent (in the absence of measurement error).

In order to justify the above statements, the following sections will first show a derivation of a form of the Koschmieder equation, the equation associated with classically defined visibility. Next will be a derivation of how visibility may be determined from measurements of apparent contrast of targets of opportunity using the HSI. Finally, the difference between the current and proposed equations is discussed.

4.3.1 Derivation of The Koschmieder Equation

To derive Koschmieder's Equation, this section starts with the definitions of radiance and contrast, then discusses the definition of visibility, and show how this leads to the desired equation for visibility.

Radiance

The apparent radiance of a target, as measured from range r , is given by

$$iL_r(\theta, \phi) = iL_0(\theta, \phi) T_r(\theta) + pL_r(\theta, \phi) \quad (4.2)$$

where

- $iL_r(\theta, \phi)$ = apparent radiance of the target from a range r with look-angle θ, ϕ
- θ = zenith angle of the path of sight
- ϕ = azimuth angle of the path of sight
- $iL_0(\theta, \phi)$ = the inherent radiance of the target, i.e. the radiance measured from a range 0
- $T_r(\theta)$ = the beam transmittance of the path of sight
- $pL_r(\theta, \phi)$ = the path radiance of the path of sight

These terms are discussed in more detail in Duntley, (1957). The first term represents that fraction of the inherent radiance which reaches the observer at range r . The second term, the path radiance, represents the radiance from the surround, scattered into the path of sight by the atmosphere along the path of sight. It is the radiance which would be observed if a target were totally black.

As discussed in detail in Duntley, (1957), these terms are exact for monochromatic radiance, however small error is introduced by using the photopic passband associated with human vision. (The photopic has a passband of 100 nm, centered at 555 nm. The HSI utilizes a filter with a passband of 70 nm, centered at 550 nm.) For convenience, a short-hand representation for Eq. 1, will be used, as given below.

$$iL_r = iL_0 T_r + pL_r \quad (4.3)$$

Contrast

A term of importance in visibility theory is the universal contrast of a target with respect to its background. The contrast from range 0 is defined as the inherent contrast, given below.

$$C_0 = \frac{iL_0 - bL_0}{bL_0} \quad (4.4)$$

Similarly, the apparent contrast, measured from range r , is given by

$$C_r = \frac{L_r - bL_r}{bL_r} \quad (4.5)$$

To begin the derivation of the Koschmieder relation, one substitutes the expression for apparent radiance (Eq. 4.3) into that for apparent contrast (Eq. 4.5), then simplifies and regroups the expression, as shown below.

$$C_r = \frac{L_r - bL_r}{bL_r} = \frac{[L_o T_r + pL_r] - [bL_o T_r + pL_r]}{bL_r}$$

$$= \frac{T_r}{bL_r} (L_o - bL_o) = T_r \frac{bL_o}{bL_r} \frac{(L_o - bL_o)}{bL_o} \quad (4.6)$$

Substituting the expression for inherent contrast (Eq. 4.4), this then becomes the following equation for apparent contrast of the target.

$$C_r = T_r \frac{bL_o}{bL_r} C_o \quad (4.7)$$

This is an expression for the apparent contrast of any target as viewed against any background.

Visibility

The WMO defines visibility as follows: "Meteorological visibility by day is defined as the greatest distance at which a black object of suitable dimensions, situated near the ground, can be seen and recognized, when observed against a background of fog or sky." (Quoted from Gordon 1979). As will be shown, under these idealized conditions, a human determination of visibility approximates a measure of the atmospheric transmittance.

Idealized Conditions

Now consider what happens if the idealized conditions implied by the WMO definition are met. First, if the path of sight is horizontal, and optically uniform, and the background is a clear sky horizon radiance, then the background radiance is the equilibrium radiance (Duntley, 1957). Under these conditions, as discussed in Duntley 1957, the apparent background radiance equals the inherent background radiance. Equation 4.7 then becomes

$$C_r = C_o T_r \quad (4.8)$$

which is a form of the Koschmieder equation applying to targets of any inherent contrast (Middleton, p. 70, 1952).

Secondly, if the target is precisely black, i.e. with radiance equal to 0, then from Eq. 4.4 it may be seen that C_o becomes -1. Since the human visual threshold is dependent only on the magnitude and not the sign of the contrast, a C_o value of 1 may be substituted into Eq. 4.8. The equation thus becomes

$$C_r = T_r \quad (4.9)$$

The Resulting Koschmieder Equations

It is useful to define the transmissivity T , which is the transmittance over unit distance. (Douglas and Booker, 1977). Since the transmittance T_r over range r is related to transmissivity T by

$$T_r = T^r \quad (4.10)$$

equation 4.9 becomes

$$C_r = T^r \quad (4.11)$$

To relate this equation to the psychophysically defined visibility, one may note that the human detection of objects against the horizon is dependent on the apparent contrast of the object. That is, there is a human contrast threshold ϵ , which depends on a number of factors such as target size, as discussed in Gordon 1979. If one defines the visibility as the range at which the contrast of the black target against the horizon sky approaches this contrast threshold ϵ , then one may let r go to V in Eq. 4.11, as the apparent contrast goes to threshold. The equation then becomes

$$\epsilon = T^V \quad (4.12)$$

which is another form of the Koschmieder equation (Douglas and Booker, p. 4-2, 1977).

This form of the Koschmieder equation may be considered a definition of visibility. It corresponds with the psychophysical definition given above, and is the relation classically used by sensor systems such as point scatter meters and nephelometers. The WMO recommends using a threshold value ϵ of .05 (Douglas and Booker, 1977).

4.3.2 Determining the Visibility from Measured Apparent Contrast

Visibility as a Function of Transmissivity

Using Equation 4.12 as a definition of visibility, one may convert the expression by taking the log of both sides, to yield an expression for visibility

$$V = \ln \epsilon / \ln T \quad (4.13)$$

Measured Transmissivity

The HSI is used to measure the apparent contrast of a near-black target with respect to the horizon. The target does not have inherent contrast of -1, so we cannot make the assumptions made earlier. Consider Eq. 4.7, repeated below.

$$C_r = T_r \frac{hL_r}{hL_o} C_o \quad (4.14)$$

The background is still the horizon (since the contrast of the target with respect to the horizon is used). But the inherent contrast is not -1. Therefore the equation describing the apparent contrast measured by the HSI is

$$C_r = C_o T_r = C_o T^r \quad (4.15)$$

This apparent contrast is measured at some range r , not equal to visibility. The apparent contrast in general does not equal the contrast threshold. However, by knowing the range and the inherent contrast, this measurement of the apparent contrast may be used as a measure of the transmissivity, as follows. From Eq. 4.15, we have

$$\frac{C_r}{C_o} = T^r \quad (4.16)$$

for the HSI measurement, from which

$$\ln \left(\frac{C_r}{C_o} \right) = r \ln T \quad (4.17)$$

which yields an expression for the transmissivity,

$$\ln T = \frac{1}{r} \ln \left(\frac{C_r}{C_o} \right) \quad (4.18)$$

This shows how the transmissivity of the atmosphere may be determined from the measured apparent contrast of a non-black target, with respect to the horizon, at range r .

Resulting Expression for Visibility from Measured Parameters

Now, this measured transmissivity may be substituted directly into the defining equation for visibility, Eq. 4.13, to yield

$$V = \frac{\ln \epsilon}{\frac{1}{r} \ln \left(\frac{C_r}{C_o} \right)} \quad (4.19)$$

or

$$V = r \ln \epsilon / \ln \left(\frac{C_r}{C_o} \right) \quad (4.20)$$

This shows how the classically defined visibility may be determined from the HSI measurements.

4.3.3 Relationship between the Proposed and Current Equation

The current equation may be derived by using a pseudo visibility, that is by replacing Eq. 4.12 with the equation

$$\frac{\epsilon}{C_o} = T^{V'} \quad (4.21)$$

This is equivalent to using Eq. 4.8, rather than 4.9. This defines the range at which the apparent contrast of the non-black target reaches a human threshold contrast.

Thus this pseudo-visibility V' is the greatest distance at which a NON-black object of suitable dimensions, situated near the ground, can be seen and recognized, when observed against a background of fog or sky. It is somewhat less than the visibility, depending on how non-black the target is. For a gray object of 0.8 inherent contrast, V' is 7% less than the visibility. (V' is not equivalent to the visual range to the target, unless the target is large and seen against the horizon sky.)

The proposed equation (Eq. 4.1 or 4.20) is not target dependent (in the absence of experimental error), and is consistent with the definition of visibility. The current equation (Eq. 2.2) represents what a human might estimate for visibility if viewing large non-black targets against the horizon. The proposed equation represents what a human might estimate for visibility if viewing large black targets against the horizon. Thus, if the shift is made to the proposed equation, the HSI will be more self-consistent, and more consistent with visibility as defined by the WMO, but less consistent with human estimates made with non-ideal targets.

5. RELATED STUDIES

Whereas the development work on this contract was directed primarily toward improvement of the visibility capability, related work in the cloud determination capability, funded under separate contract, resulted in developments which are directly applicable to the HSI/WSI composite system. The first of these related efforts was development of an improved cloud detection algorithm for the WSI (Kochler, et al, 1991), and the second was

development of a night-capable WSI system (Shields, et al, 1991).

5.1 Directional Cloud Decision Algorithm

As discussed in Section 2.2, the WSI data undergo several processing steps to yield a cloud decision image, in which opaque cloud, thin cloud, and clear sky are identified. Several calibrations are applied in this process, and then a red/blue ratio image is generated.

This ratio image is much more appropriate than the original radiance image for use in cloud detection, for a number of reasons. It is unrealistic to use a fixed radiance threshold, because the radiance of dark clouds can be darker than the radiance of the sky. A radiance threshold would also be quite difficult, because the radiance of the background sky varies considerably over the image, and also varies significantly at different times of the day.

By using a spectral ratio, this first normalizes most of the clear sky variance over the image, as well as most of the variance as a function of time of day. It also allows a clean distinction between the dark or gray clouds and the dark blue sky. Most of the early data processing of WSI data used a ratio threshold to identify the clouds.

The opaque clouds are detected quite well through use of a fixed ratio threshold. We find that the opaque clouds have a well defined spectral signature (as measured at the two wavelengths used by the WSI), which is reasonably independent of the solar zenith angle and cloud zenith angle. The fixed ratio threshold works well under a variety of conditions, for daytime use (except near dawn and sunset), and is used in both the original algorithm and the new directional algorithm.

Thin clouds are better represented as a perturbation with respect to the background sky ratio. Even though the background sky ratio is much less variable than the sky radiance, there remains some variance over the sky. In particular, the ratio is higher near the sun and near the horizon.

Several contrail cases were studied in an effort to determine the relationship between thin clouds and their background sky conditions. We found that the ratio of thin cloud red/blue radiance ratio to the clear sky background red/blue radiance ratio remains fairly constant along sections of contrails exhibiting uniform optical properties. If the clear sky background ratio were known, a thin cloud discrimination could then be based on whether the observed ratio exceeds the background ratio, and the degree of "thinness" could be estimated by the observed/background ratio. The thin cloud decision

"problem" then becomes one of determining a reasonable estimate of the clear sky background ratio.

The red/blue clear sky ratio distribution is influenced by many factors the most important of which are the solar zenith angle, and the haze features of the atmospheric boundary layer. Figure 17 shows the variation of the ratio distribution as a function of solar zenith angle. Note how the clear sky background "whitens" (r/b ratio increases) as the sun approaches the horizon. Figure 18 illustrates the boundary layer haze influence, with the pristine February Arctic air mass yielding "bluer" ratios than the haze laden air mass from July.

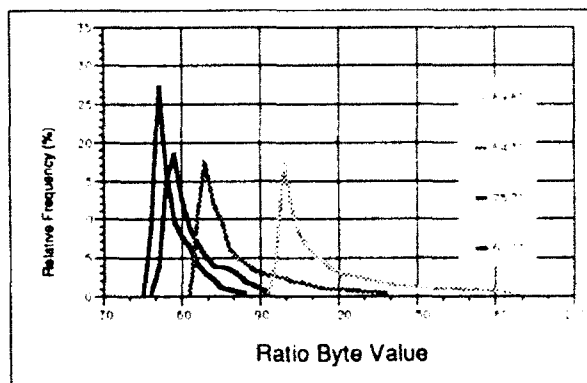


Fig. 17 Clear Sky Solar Zenith Angle Dependence:
11/Feb/89 - Columbia, MO

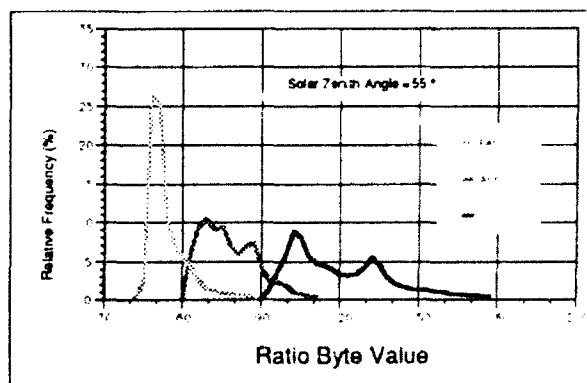


Fig. 18 Clear Sky Haze Layer Dependence:
Columbia, MO, 1989

Several approaches to modeling the background clear sky ratio were evaluated. It was determined that due to variations in mixing layer height and prevailing air mass type at different sites, it was more efficacious to use measurements of the clear sky ratio over a period of time at a given site, rather than model the clear sky ratio.

As the visibility changes, and the aerosol changes from day to day or hour to hour, the magnitude of the

clear sky ratio changes. The modeling implied that these changes are proportional for the full sky scene. That is, a change from a very clear day to a hazy day results in a nearly constant fractional change in the r/b ratio. The WSI data were used to verify that this relationship holds reasonably well over a wide range of conditions. This result allowed us to use a clear sky background which depends on the haze level, in the new cloud algorithm. In effect, this means that a sky which is white due to haze, as opposed to thin cloud, is identified as clear.

In summary, the directional algorithm first identifies the opaque clouds through a fixed ratio threshold. Then the thin clouds are identified with respect to a background clear sky r/b ratio which has been normalized for haze level.

A sample cloud decision image resulting from the directional algorithm is shown in Fig. 19. A fixed threshold algorithm would have identified the down-sun portions of this contrail as clear. The directional algorithm is quite effective in removing this directional bias.

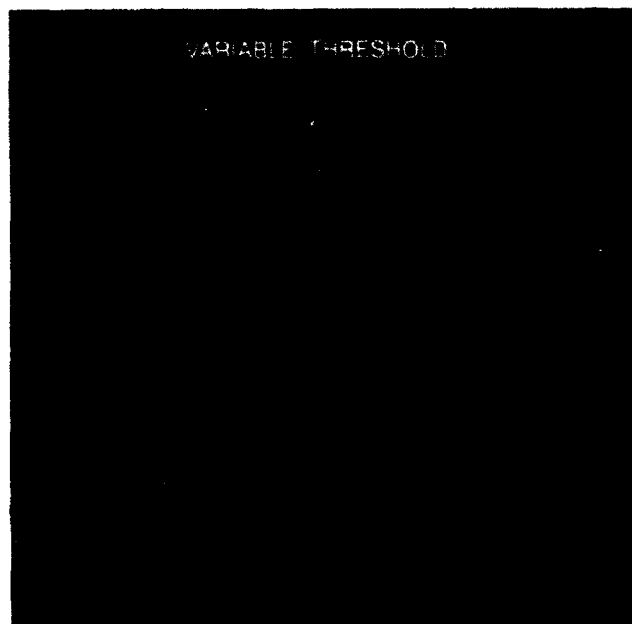


Fig. 19 Variable threshold cloud decision image

The directional algorithm has not been programmed into the composite HSI/WSI system, due to limited funding. However the conversion of the system to include this update is quite practical.

5.2 Development of the Day/Night WSI

A major accomplishment of the Optical Systems Group has been the development of a WSI system capable of acquisition of night imagery.

The Day/Night WSI takes advantage of many of the technologies used in the Day WSI. The new system includes a larger fisheye lens, with high throughput and full upper hemisphere coverage down to 90 degrees zenith angle. This enables detection of the vertical buildup on the horizon, as well as providing full coverage for comparison with the meteorological observer. It is also useful in characterizing the HSI backgrounds with respect to the presence of cloud clutter.

The Day/Night WSI uses a slow scan Charge Coupled Device (CCD) sensor to yield the additional sensitivity required for night operation. Spectral filters are used, as with the Day WSI, at least down to quarter moon conditions. A fiber optic taper is used in place of the previously used lens relay system, to resize and relocate the image plane. The Day WSI's equatorially driven solar occulter is replaced in the Day/Night system with a zenith/azimuth dual drive occulter, in order to more readily transition from sun to moon occultation and adapt to use on moving platforms.

One of the important design criteria is the large range of flux levels the system must be able to deal with. Figure 20 shows the naturally occurring illuminance levels under a variety of lighting conditions. These data are from the work of Brown 1952, and are consistent with irradiance measurements acquired by our group at the Visibility Lab over a period of several years. In Fig. 20, the daytime illuminance conditions the Day WSI has had to deal with are shown in the top two curves on the right side of the plot. These represent clear to dark storm conditions for sun zenith angles 0 to 90 degrees. The Day/Night WSI can acquire imagery at 450nm and 650nm down to quarter moon and urban starlight conditions. For rural starlight conditions, it is currently necessary to use open-hole. This represents approximately a 9 log range of lighting conditions. The sensor is designed to obtain the necessary sensitivity range by using the approximately 3-4 log sensitivity of the camera chip, 2-3 logs range from exposure control, and 2-5 logs range through neutral density filter control.

Two sample night images are shown in Fig. 21. Those images were acquired in San Diego. Fig. 21a was acquired under starlight (no moon) conditions, with a 25 second exposure. Flux levels were quite adequate. Fig. 21b was acquired under moonlight. Only the more dense portions of the cloud layer were visually detected at the time.

One of the Day/Night WSI units has been fielded in New Mexico, and is acquiring very high quality data. The night cloud decision algorithms are in development

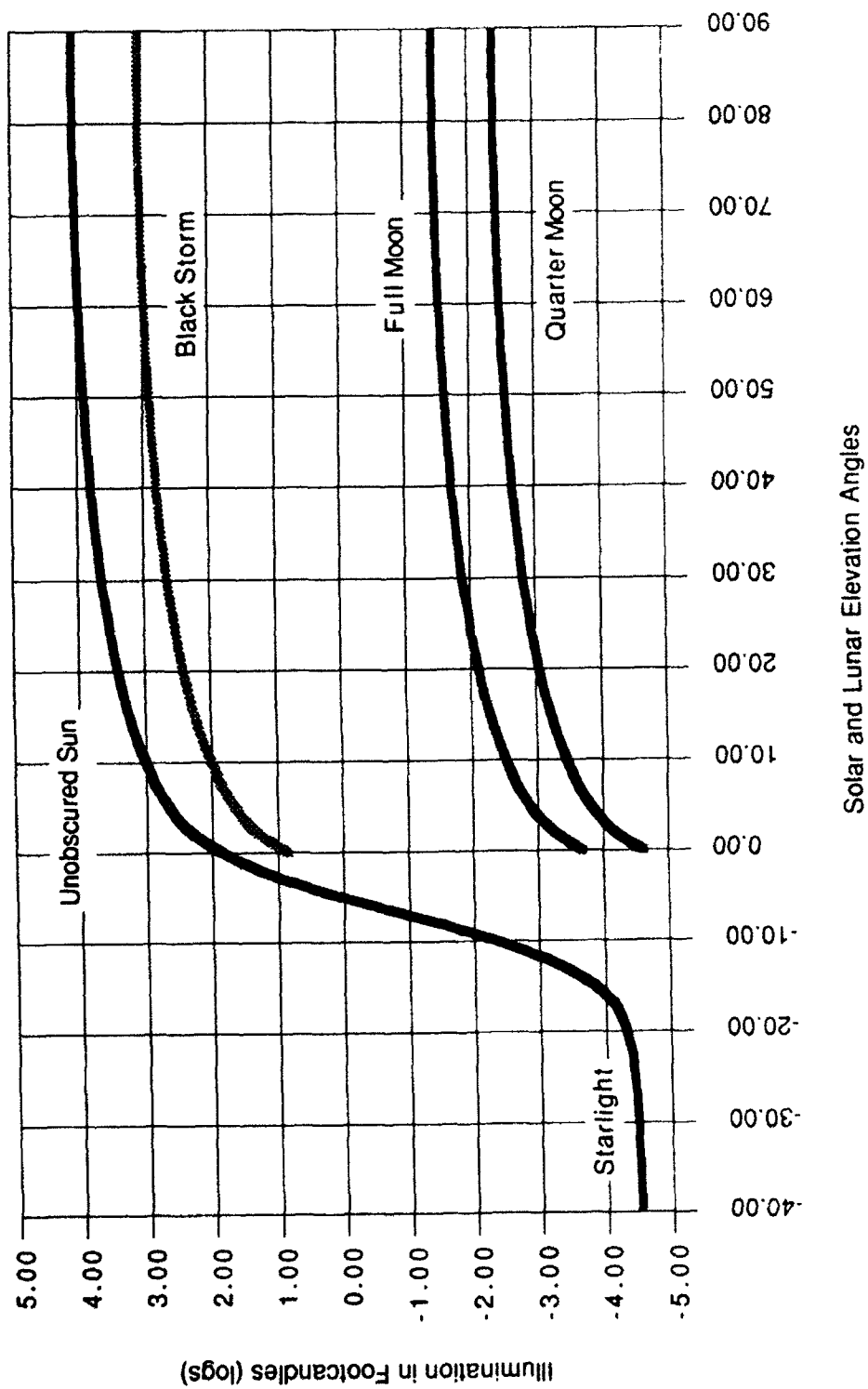


Fig. 20 Natural Illumination Levels. These measurements, from Brown 1952, illustrate flux conditions the Day/Night WSI should encounter.



a) Starlight (no moon) conditions.
11 Sep 91, 25 seconds integration



b) Moonlight conditions.
18 Sep 91, 30 seconds integration

Fig. 21 Sample Night Sky Images from the Day/Night WSI

at this time. The Day/Night WSI has many applications, potentially including the automated weather system for which the composite HSI/WSI system was developed.

6. RECOMMENDATIONS

The Composite HSI/WSI is a very capable, unique system applicable to both research applications and auto-

mated weather systems. In spite of its high degree of current capability, there remain several areas of development which hold significant potential.

The first potential development area to be discussed below is conversion of these systems into tactical systems, or more generally to small, relatively inexpensive systems which could be applied by a broader user base. The second development area has to do with improvement of the quality and capabilities of the current system. These include further development and testing of the night visibility capability, and improvements in both the visibility and cloud algorithms. The third development area involves combining both systems into one optical system capable of determining not only cloud cover, visibility, and radiance distribution, but directional terrain reflectance as well. These three areas of research and development are discussed in the following sections.

6.1 Compact and Ruggedized Systems

In order to make the WSI and the HSI more available to both the research community and the tactical military community, it is highly desirable to develop versions of these instruments which are smaller and less costly. It is important that such systems require minimal intervention by personnel highly trained in the engineering of the systems. The WSI and HSI units have been operational for several years; development of compact, tactical versions of these units is both feasible and appropriate at this time.

6.1.1 A Compact WSI System

In order to create a compact version of the WSI, we must consider the sensor, the controller, and the power requirements. Up to this point, the sensor has consisted of a single solid state camera (CID in the Day WSI, and a slow scan CCD in the Day/Night WSI), with a filter changer, aperture control, fisheye and relay optics, and occulter.

It should be feasible to miniaturize this combination primarily through use of a color camera, to acquire the necessary imagery. In order to evaluate this possibility, the Optical Systems Group has performed tests of a 3-chip color camera, acquiring imagery of clouds and sky. We determined that it is possible to extract the red and blue components of the color image separately, and ratio them just as one would the red and blue images acquired with the current image.

If the Compact WSI makes use of such a color camera, it should not be necessary to use a filter changer. Additionally, since the color images would be acquired simul-

taneously, rather than in separate grabs 2 seconds apart, use of an auto iris becomes practical in the compact WSI. The color camera does not have the same flexibility in control of the filter choices, however it has the advantage of compact size. Also, due to simultaneity of the color image acquisitions, applications in quickly changing environments, such as onboard an aircraft, become more practical.

There are a variety of camera choices, depending on the desired trade-off between resolution and cost. The color camera used in the above tests yielded full 512 x 512 images independently in each color (RGB), to yield resolution equivalent to that of the current WSI. Less costly cameras are available at lower resolution.

Without the need for spectral filters and computer control of the aperture, much of the requirement for interface between the computer and sensor is relieved. If in addition the occulter is independently controlled through a small programmable device (micro controller), this eliminates the need for much of the logic and mechanical control inherent in the current system.

It is possible to further decrease the size of the control hardware by taking advantage of the significant progress which has been made in recent years in combining a variety of functions on a single computer board. With a configuration much like the current lap-top computers, possibly with a single image board added, it should be possible to enable the most basic capabilities of the current WSI with a much smaller computer system.

Cooling remains in issue for the compact WSI, however with a much smaller sensor package to keep cooled, it should be feasible to convert from the large chiller system currently in use to a smaller cooler such as a thermo-electric system. This conversion of the cooling system would also minimize the power requirements of the full system.

The WSI system is currently quite intensive in its requirement for interaction of trained personnel. This interaction ranges from radiometric calibration, and analysis of the calibration results, to evaluation of the clear sky background used in the directional algorithm. Regarding the calibrations, the primary calibrations involved are image size and flux control calibrations, linearity, and red/blue relative radiance calibrations.

With the compact sensor package discussed above, the first two of these calibrations would no longer be required. An automatic in-field calibrator would be developed to test the linearity and relative spectral response. Following initial calibration and setup, the

calibration could then be automatically updated in the field at 3-month intervals (or as required) with the in-field calibrator.

Regarding evaluation of the clear sky background, this evaluation is necessary only for the thin cloud algorithm. As a first approach, the system could be trained to identify only opaque clouds. For thin clouds, if one can accept lower resolution than that used in the current WSI system, there are several possible algorithms which may prove to yield adequate thin cloud detection.

Thus both the WSI hardware and software have matured to the point that development of a compact, more transportable system is very feasible. The tactical military application is an obvious candidate for use of such a system. Likewise, availability of these units for a variety of research application would be highly desirable.

6.1.2 A Compact HSI System

The development of a compact HSI unit would appear to require more technical compromises than required for development of a compact WSI unit. The scheme currently used in the HSI, measurement of the apparent contrast of a dark target with respect to the sky, requires a high resolution image. The HSI uses a very high angular resolution rotary table, in order to access the full 360 degree surrounding horizon with the small field of view optics, acquiring many images at representative azimuthal points. The rotary table is probably not practical to compartmentize at this point.

A reasonable technical compromise between the need to eliminate the rotary table and the need for tight angular control is the use of a hand held, narrow field of view optical system with crosshairs. A user would point the crosshairs at a dark target of interest, acquire the image, and then acquire the image of the horizon sky. The system could then automatically compute the visibility in that azimuthal direction. This would require that the user input an estimate of the range to the target.

With this approach, the automation of the HSI is sacrificed in return for a convenient, transportable unit. The resulting visibilities should be reasonably accurate, if an accurate range to the target is input.

A second approach to determination of visibility is to use the same optical system used for the WSI (either the current or the compact). The shape and magnitude of the clear sky background ratio provides a great deal of information related to the visibility and height of the inversion layer. The current cloud algorithm makes use of the nearly proportional relation between visibility and

the magnitude of the clear sky background ratio at a given site. Our group, previously at the Visibility Lab, has done experimental work with this inversion technique in the past; see Gordon (1985).

Thus a tactical visibility sensor seems reasonable to evaluate, however it may not be possible to retain the automated capability in a small tactical visibility device based on the HSI.

6.2 Improvements of Quality and Capability of the Current HSI/WSI

Even if development of a compact WSI and/or HSI system comes to fruition, the current system remains a valuable complement as a high accuracy research instrument. In this mode, the instrument may be used for making precision measurements for model evaluation, as well as in support of test sites. There are several areas of potential improvements, which will only be summarized here, since they have been discussed earlier in this report.

6.2.1 Integration of the Sensitivity Study Results

As discussed in Section 4.2, a sensitivity study revealed several areas of potential improvement to the system. Of these, the most significant were probably as follows. The linearity of the camera should be measured and applied to the imagery on a routine basis. The horizon region of interest should be evaluated for cloud clutter, so that clear horizon is used. And a better range of targets should be used, with a sorting algorithm that gives more preference to those targets expected to yield accurate results.

6.2.2 Addition of the Directional Algorithm

As discussed in Section 5.1, a more accurate directional cloud algorithm has been developed under separate funding, which applies to WSI data. The current composite system contains the older code, based on a fixed ratio threshold. This technique is quite accurate for opaque clouds (if the proper calibration inputs are up to date), however it tends to under-estimate the down-sun thin cloud amount. Up to this point, the directional cloud algorithm has required some analyst intervention in the selection of the haze normalization. As this selection process becomes more automated, it becomes appropriate to convert the logic in the composite system to include the directional cloud algorithm, thus resulting in more accurate thin cloud assessment.

6.2.3 Further Development of Night Visibility

During this year, theoretical analysis was developed which showed how to determine visibility from measure-

ments of lights of opportunity at night (Section 3.2). Programs were developed to allow the acquisition of test data (Section 3.4), and the data yielded reasonable results (Section 3.6). However an evaluation of the camera performance indicated that the camera currently used in the system should be replaced for night applications (Section 3.5).

We recommend that an evaluation of alternate camera sensor choices should be made, after which further development of the automated night visibility capability can proceed. This development should include an error analysis of the proposed theoretical methods, programming of the selected method, and evaluation of engineering considerations such as the stability of available light sources.

6.3 A 220 Degree Whole Sky Imager

A super wide angle version of the WSI that presently is under consideration at MPL would use a 220 degree field of view super fisheye lens which is currently available. Thus the full scene would include the overhead sky dome, the local horizon, and the surrounding terrain. Output products related to cloud cover would be produced in a manner similar to that used in the current WSI systems.

In addition, bi-directional surface reflectance data may be derived from the composite sun-sky-surface radiance measurements. Our experience to date with the Nikkor 8 mm fisheye used in the Day/Night WSI (EO Camera 6) illustrates outstanding image quality and angular resolution right up to the outside edge of each image. Assuming equal quality in the Nikkor 6mm superfisheye, the detection and identification of horizon targets and nearby surface features should enable the extraction of the desired surface radiance. The 512 x 512 chip would yield about 0.4 degrees per pixel, and 0.2 degrees per pixel may be obtained with the use of a 1024 x 1024 chip.

In addition to cloud cover, sky radiance, surface radiance, and surface reflectance properties, this system has potential for determination of the visibility. Initial experimental evaluation of proprietary techniques for zooming into selected subsets of the image has yielded positive results. By zooming into selected regions near the horizon, application of algorithms much like those used in the HSI may become feasible. Thus this 220 degree system has tremendous potential for a variety of applications requiring characterization of the atmosphere/surface radiative and meteorological properties.

7. SUMMARY

The Automated Observing System combines the capabilities of the Whole Sky Imager for cloud field assessment, and the Horizon Scanning Imager for determination of the sector visibility. During the past funding interval, much of the effort on this system was directed toward development of night visibility capability. A theoretical development of the equations and analytic approaches to night visibility has been completed. The derived equations allow one to rigorously derive the visibility from measurements acquired at night with the system.

A variety of hardware and software adaptations have been completed. These include building the electronics necessary to enable acquisition of imagery with multiple integration periods. This change required extensive software changes, as well as use of a new image board. As a result of the lack of downward compatibility in the image boards, significant work to adapt the Day WSI and HSI code to the new image board was also required.

Test and calibration data indicate that the system is working reasonably normally, although the aging characteristics of the CID camera appear to make it unsuitable for night visibility. We recommend conversion of the system to a more sensitive CCD. System performance was adequate, however, to test the night visibility scheme. The results of the test were very positive, yielding appropriate values for visibility at night. Additional work in the automation of this technique, as well as error analysis, is recommended.

During this period, an in-depth sensitivity analysis of the daytime visibility system was completed. Several areas for improvement of the day visibility determinations were identified.

Our recommendations include further development of the above issues. In addition, we feel that the system has evolved to the point that development of a tactical system for cloud cover and possibly visibility is both feasible and appropriate. Such a system could be portable and compact, and run on batteries, to provide measurements of opaque and thin cloud cover.

8. ACKNOWLEDGMENTS

The authors would like to thank H. Albert Brown of Phillips Laboratory for his support and encouragement in the development of this system. We are indebted to the following members of the Marine Physical Laboratory for their outstanding efforts and contributions: Carole Robb for document preparation, Harry Sprink for hard-

ware revisions, Tom Koehler for many helpful discussions, Wayne Hering for his early work in the previously reported development of the Day HSI, and Jack Varah for his work in sensor evaluation and testing.

9. REFERENCES

- Douglas, C. A., and R. L. Booker (1977), *Visual Range: Concepts, Instrumental Determination, and Aviation Applications*, U.S. Department of Transportation, Federal Aviation Administration, Systems Research and Development Service, Report No. FAA-RD-77-8, Washington, D. C. 20590.
- Duntley, S. Q., A. R. Boileau, and R. W. Preisendorfer (1957), *Image Transmission by the Troposphere I*, University of California, San Diego, Scripps Institution of Oceanography, JOSA 47, 499-506.
- Federal Meteorological Handbook No. 1 (1988), *Surface Observations*, U.S. Department of Commerce, National Oceanic and Atmospheric Administration, Washington, D.C., FCM-H1-1988.
- Gordon, Jacqueline I. (1979), *Daytime Visibility, A Conceptual Review*, University of California, San Diego, Scripps Institution of Oceanography, Visibility Laboratory, SIO Ref. 80-1, AFGL-TR-79-0257, ADA085451.
- Gordon, Jacqueline I. (1985), *New Uses for the Solar Almucantar*, Applied Optics Vol 24, 3381-3389.
- Gordon, Jacqueline I. (1989), *Nighttime Visibility*, Viz. Ability, Inc., 2941 Corvallis, OR 97330-1255, VA189-1.
- Johnson, R. W., M. E. Karr, and J. R. Varah (1990), *Automated Visibility Measurements with a Solid-State Imager*, University of California, San Diego, Scripps Institution of Oceanography, Marine Physical Laboratory, SIO Ref. 92-34, PL-TR-91-2016, ADA246892.
- Johnson, R. W., W. S. Hering, and J. E. Shields (1989), *Automated Visibility and Cloud Cover Measurements with a Solid-State Imaging System*, University of California, San Diego, Scripps Institution of Oceanography, Marine Physical Laboratory, SIO Ref. 89-7, GL-TR-89-0061M, ADA216906.
- Johnson, R. W., J. E. Shields, and T. L. Koehler (1991), *Analysis and Interpretation of Simultaneous Multi-Station Whole Sky Imagery*, University of California, San Diego, Scripps Institution of Oceanography, Marine Physical Laboratory, SIO Ref. 91-33, PL-TR-91-2214, ADA253685.

- Koehler, T. L., R. W. Johnson, and J. E. Shields (1991), *Status of the Whole Sky Imager Database*, University of California, San Diego, Scripps Institution of Oceanography, Marine Physical Laboratory, Proceedings of the Cloud Impacts on DOD Operations and Systems, 1991 Conference.
- Middleton, W. E. K. (1952), *Vision through the Atmosphere*, University of Toronto Press.
- Shields, J. E., R. W. Johnson, and M. E. Karr (1991), *A Sensitivity Study of Daytime Visibility Determination with the Horizon Scanning Imager*, University of California, San Diego, Scripps Institution of Oceanography, Marine Physical Laboratory, SIO Ref. 91-15, PL-TR-91-2189.
- Shields, J. E., R. W. Johnson, and T. L. Koehler (1991), *Imaging Systems for Automated 24-Hour Whole Sky Cloud Assessment and Visibility Determination*, University of California, San Diego, Scripps Institution of Oceanography, Marine Physical Laboratory, Proceedings of the Cloud Impacts on DOD Operations and Systems, 1991 Conference.
- Varah, J. R., and H. G. Sprink (1991), *Charge Injection Device Integration Control Circuit*, University of California, San Diego, Scripps Institution of Oceanography, Marine Physical Laboratory, Optical Systems Group Technical Note No. 233.